ENERGETICS, MAXIMUM POWER AND MAXIMUM EFFICIENCY REGIMES OF A MICROSCOPIC HEAT ENGINE

A Thesis Submitted to the School of Graduate Studies of
Addis Ababa University

In partial Fulfilment of the Requirements for the
Degree of Master of Science in Physics

By

Demmelash Hailu

Addis Ababa, Ethiopia

June 2006.

ADDIS ABABA UNIVERSITY
FACULTY OF SCIENCE
DEPARTMENT OF PHYSICS

The undersigned hereby certify that they have read and recommend to the Faculty of Science School of Graduate Studies for acceptance a thesis entitled "**Energetics, Maximum Power and Maximum Efficiency Regimes of a Microscopic Heat Engine**" by **Demmelash Hailu** in partial fulfillment of the requirements for the degree of **Master of Science in Physics**.

Dated: July 2006

Name	Signature
Dr. Mulugeta Bekele, Advisor	_______________
Dr. Mesfin Asfaw, Examiner	_______________
Dr. S. K. Goshal, Examiner	_______________

To My parents

Acknowledgements

My warmest appreciation must go to Dr.Mulugeta Bekele, my instructor and advisor, for his unreserved help. in addition to exposing to good research atmosphere and guiding me, he followed up my permeance continuously and gave me appreciable comments. His friendly approach enabled me to deal with him easily and to share his long research experience. The day to day fruitful discussions I had with him inspired me lots to be engaged in research activities in the future so that I give special credit to him. I would like to thank him once again.

I am very grateful to my brother Endeshaw Hailu for all his unlimited help and support during my study. He encouraged me to join the School of Graduate Studies of AAU. Moreover, he covered all my financial needs including tuition fees and contributed lots in providing me with different materials. I had continuous discussions with him from the beginning to the end of my MSc work and got feedbacks which helped me lots to improve my study. He also read this thesis critically and gave me highly valued comments.

I am indebted to W/t Meseret Tadesse for her help in typing my thesis and w/t Achamyelesh Duressa for her special help. I admire the discussions I had with my colleagues: I would like to thank all of them.

I would like to extend my thanks to my parents, brothers, sisters and friends for their encouragements.

My thanks are also to Dr. Mesfin Asfaw who read this thesis and gave me valuable comments and the departments physics and ths School of Graduate Studies, AAU, for all kinds of cooperation they provided me.

Addis Ababa, Ethiopia Demmelash Hailu

June 2006.

Abstract

A microscopic heat engine is modeled as a Brownian particle which moves through a highly viscous medium, in an alternately placed hot and cold heat baths, in a periodic asymmetric saw-tooth potential. Expressions for unidirectional probability current density (due to thermal variation) as well as energetics of the engine are found in terms of parameters of the engine for two cases: in the presence and absence of static external force. Power output and efficiency at maximum power and maximum efficiency regimes are studied numerically for both cases.

Table of Contents

List of Figures

Chapter 1

Introduction

Of the four basic papers Albert Einstein published in 1905, his publication on the theory of Brownian motion plays central role in the modern studies of stochastic systems in which fluctuations govern the dynamics at micro-scale and even at nano-scale. Noise or fluctuations can arise either from the interaction of systems with external world or from thermal bath. Commonly, fluctuations which arise from either source is considered as undesired effects. However, at molecular scale, fluctuations have played significant constructive role for the development of the ongoing nano-technology [1, 2, 3].

Biological systems which transduce chemical energy available in the form of ATP into useful work (hydrolyzing ATP molecule) has motivated many researchers to study physics of activated processes [4]. At molecular level, biological systems transduce chemical energy obtained from chemical reaction out of equilibrium into mechanical work, to induce directed motion in a very noisy environment with high efficiency against concentration or potential gradients [5, 6]. Among molecular motors, kinesin (responsible for the movement of proteins and vesicles within cells) and myosin (responsible for muscle contraction) are most extensively studied experimentally at the level of individual molecule using nano-tools such as optical or magnetic tweezers, atomic-force-microscope, etc., [7, 8].

Different physical models called Brownian ratchets have been developed to study the dynamics of systems in a fluctuating periodic system. Flashing ratchets (periodic potential is allowed to fluctuate with finite time correlation between two states characterized by different barrier heights), rocking ratchets (asymmetric potential) and inhomogeneous ratchets (space dependent diffusion coefficient D(x) $= \frac{k_B T(x)}{\gamma(x)}$) are some of them. In general, Brownian ratchet models are systems with an underlying spatially asymmetric periodic potential, that exploit the non-equilibrium fluctuations presented in the medium, to induce a directed motion at microscopic level. They represent physical analogue of bio-molecular motors that also work out of equilibrium to induce intercellular transport [1,2, 9].

In spite of spatial asymmetry in the potential, if the system is isolated and kept in isothermal environment, particle in a ratchet can not diffuse in any preferential direction. Isothermal systems are full of noise but the validity of the principle of detailed balance does not allow extracting useful work from such systems [9, 10]. For systems which are in equilibrium with thermal bath, according to the principle of detailed balance, the rate of forward motion is equal to the rate in the backward direction so that there is no preferential direction of flow for the particle current. Therefore, to extract useful work from fluctuations it is a must that the system should be driven out of equilibrium. In other words, it is never possible to construct heat engines that use fluctuations from thermal energy from a single heat bath to do mechanical work. R. Feynman showed this situation using an engine consisting of a ratchet and a pawl subjected to thermal fluctuations [11] even though his engine has some misguided aspects as criticized by Parrondo and his coworkers [12]. But, in the presence of non-equilibrium fluctuations the principle of detailed balance does not hold any more. Hence, the particle starts to move in a preferential direction, generally. Thus, both non-equilibrium fluctuations and spatial or temporal asymmetry in potential conspire to induce a unidirectional flow in the absence of bias [13].

Langevin or Fokker-Plank formalisms are used to study stochastic dynamics. The effect of thermal environment is modeled by considering randomly fluctuating force (Langevin force) $\xi(t)$ and the coefficient of viscosity γ which are related through the fluctuation dissipation theorem, i.e., $\langle\xi(t)\xi(s)\rangle = 2\gamma k_B T\delta(t-s)$ such that the random noise $\xi(t)$ satisfies $\langle\xi(t)\rangle = 0$. The inertial term is dominated by these two terms at microscopic level so that it is negligible [14, 15].

Various physical quantities like efficiency of energy conversion, input energy, work done, energy dissipation, entropy production, etc., can be obtained in stochastic processes where physical quantities are known in terms of their probability distribution. The important quantity that has got considerable attention in the study of Brownian ratchets is the energetic efficiency with which a Brownian ratchet converts fluctuations into useful work. The usefulness of any engine is measured in terms of the extent of work that can be extracted efficiently out of it [7, 14, 16-20]. The molecular motors in living cells are found to be highly efficient in their noisy environment. For example, kinesin is about 60 percent efficient [21] and F_1-ATPase, which is responsible for generating ATP from the flow of protons across the mitochondrial membrane found to be nearly 100 percent efficient experimentally [8].

For the ratchet to perform work usually a small force (load) has to be applied opposite to the direction of current in the ratchet. Then, the particle keep on moving, on the average, against the load doing work by converting part of the input energy into mechanical energy.

Many inherently noisy processes in a cell are carried out by very few number of molecules. The way the cell manages to coordinate these noisy processes is one of the remarkable and still poorly understood facts of complex biological processes. How do microscopic cell machines operate? How is their operation affected by large fluctuations in which they work? Can we build man-made nano-devices with similar properties? and so on are questions that people have been worried about. A great challenge for the ongoing nano-technology is the design and construction of microscopic motors that can use input energy to drive directed motion in the face of inescapable thermal and other fluctuations. Consequently, there has been an increased interest in the study of small systems (dimensions of few nanometers) which are found through out physics, chemistry, biology, etc. These small systems have underlying size-dependent properties. Hence, understanding these properties is one of the most interesting areas of research currently [22-27].

Researches in Brownian motors could lead to nano-scale applications such as molecular sievers, molecular pumps, transistors and even micro-sized factories that assembles motors to be used in microscopic surgery.

Hernández and his coworkers [28] studied optimal operation modes for Fenman engine. In particular they took power and efficiency as their objective functions and investigated them in terms of different parameters characterizing Feynman engine. They showed the regions in which the Feynman engine operates between maximum power and maximum efficiency regimes numerically. Being inspired by their work on Feynman engine, we intend to model a microscopic heat engine and study its energetics and region of operations between maximum power and maximum efficiency regimes.

The aim of this thesis work is to propose a model and then to study the energetics and optimization of a microscopic heat engine (engines that use local temperature gradients in asymmetric potentials to move particles against an external load) giving particular attention to probability current density, power and efficiency of the engine. The thesis work is organized as follows: in Chapter 2 a model for microscopic heat engine in the absence of external load will be presented. Then, analytic expressions for probability current density, power output and efficiency will be found and the influence of model parameters on these quantities will be investigated. In particular, maximum power and maximum efficiency regimes are studied numerically. In Chapter 3 we modify our model by introducing an external static force which acts against the flow of current and re-consider the quantities mentioned in Chapter 2 such as unidirectional current, power, efficiency and so on. Summary and conclusion is given in Chapter 4.

Chapter 2

A Brownian Particle in Ratchet Potential out of Thermal Equilibrium with Zero External Load

In this chapter stochastic model is developed for a microscopic heat engine. A Brownian particle in a periodic but asymmetric sawtooth potential without load moving in a highly viscous medium whose temperature, with the same period as the potential, varies spatially is used to model the heat engine. In the first section of this chapter we develop a stochastic model and discuss its equation of motion. In the second section the steady state probability current density of the Brownian particle is found using periodic boundary condition, continuity of the steady state probability density and normalization of the steady state probability density. Then, in the next two sections the stochastic energetics, the maximum power regimes and the maximum efficiency regimes are found in terms of the parameters used to describe the model. The maximum power regimes and the maximum efficiency regimes are examined numerically.

2.1 Stochastic Model and Equation of Motion

Consider a Brownian particle in a highly viscous medium moving along one dimensional asymmetric saw-tooth potential of period L, ($L = L_1 + L_2$), and barrier height, U_o, which is subjected to a temperature that changes in space between hot and cold values periodically with period L (see Fig. 2.1 below). The potential and the temperature profiles are given by

$$U(x) = \begin{cases} \frac{U_o}{L_1}x + U_o & \text{for } -L_1 < x \leq 0 \\ \frac{-U_o}{L_2}x + U_o & \text{for } 0 < x \leq L_2, \end{cases} \tag{2.1.1}$$

and

$$T(x) = \begin{cases} T_h & \text{for } -L_1 < x \leq 0, \\ T_c & \text{for } 0 < x \leq L_2 \end{cases} \tag{2.1.2}$$

respectively, where T_h is temperature of hot reservoir of width L_1, T_c is temperature of cold reservoir of width L_2 as shown in Fig. 2.1 and

$$U(x + aL) = U(x),$$

$$T(x + bL) = T(x), \tag{2.1.3}$$

i.e., both $U(x)$ and $T(x)$ are periodic with the same period L, where L=$L_1 + L_2$, a and b being integers.

Consider a Brownian particle moving in a periodic asymmetric saw-tooth potential of period L with spatially varying temperature between two constant values of T_h and T_c periodically with the same period as the potential with zero externally applied force. The dynamics of the Brownian particle is governed by the Langevin equation

$$m\ddot{x}(t) + U'(x(t)) = -\gamma\dot{x}(t) + \hat{\xi}(t), \tag{2.1.4}$$

where m is mass of the particle, $x(t)$ is position of the particle, $U(x(t))$ is the potential, γ is coefficient of friction and $\hat{\xi}(t)$ is a randomly fluctuating force in the form of thermal

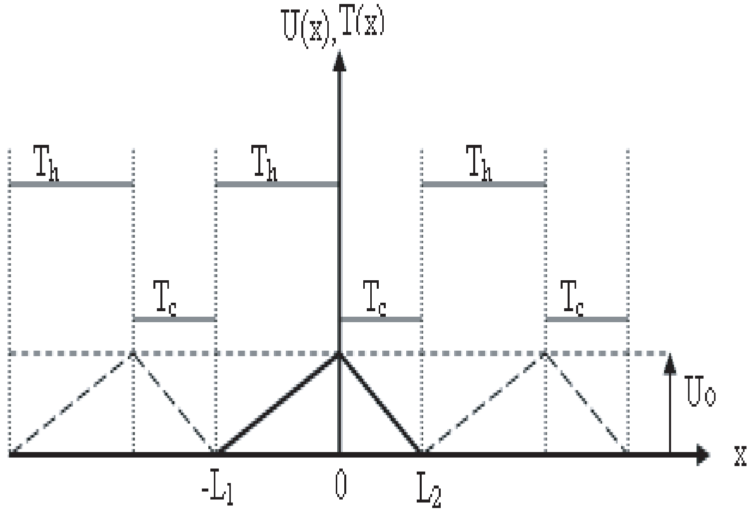

Figure 2.1: Model for microscopic heat engine: a Brownian particle placed in a periodic, asymmetric potential and periodic spatially varying temperature in the absence of external load.

noise from the heat baths (Langevin force). The random fluctuating force $\hat{\xi}(t)$ is a Gaussian white noise satisfying two conditions

$$\langle \hat{\xi}(t) \rangle = 0 \tag{2.1.5}$$

and

$$\langle \hat{\xi}(t)\hat{\xi}(s) \rangle = 2\gamma k_B T(x)\delta(t-s). \tag{2.1.6}$$

Here $\delta(t-s)$ is Dirac's delta-function, k_B is Boltzmann's constant. The coefficient of $\delta(t-s)$ in Eq. (2.1.6), which is called noise intensity, is from fluctuation dissipation theorem. Note that "dot" and "prime" represent differentiation with respect to time and space respectively through out this work.

At microscopic scale where thermal fluctuation plays significant role and in the strong friction limit the dynamics in Eq. (2.1.4) is over damped so that the inertial term $m\ddot{x}(t)$ can be neglected [1, 2, 6, 9]. Consequently, the dynamic in Eq. (2.1.4) reduces to

$$U'(x(t)) = -\gamma\dot{x}(t) + \hat{\xi}(t). \tag{2.1.7}$$

2.2 The Steady State Solution and Probability Current Density

Due to the asymmetric periodic saw-tooth potential and the temperature gradient shown in Fig 2.1, there is directed transport of the Brownian particle towards positive x direction, in general, provided that the parameters used in modeling are in the domain of interest. In this section, using the Fokker-Plank equation (FPE) corresponding to the Langevin equation (2.1.7), a steady state solution $p_{ss}(x)$ which is normalized over period L is evaluated. Then, a constant probability current density J_0 is obtained, where J_0 is to mean a constant probability current density in the absence of external load.

We can rewrite equation (2.1.7) as

$$U'(x(t)) = -\gamma\dot{x}(t) + \sqrt{2\gamma k_B T(x(t))}\xi(t), \tag{2.2.1}$$

where

$$\sqrt{2\gamma k_B T(x(t))}\xi(t) = \hat{\xi}(t), \tag{2.2.2}$$

such that

$$\langle\xi(t)\rangle = 0 \tag{2.2.3}$$

and

$$\langle\xi(t)\xi(s)\rangle = \delta(t-s). \tag{2.2.4}$$

By taking $k_B = 1$, equation (2.2.1) can be re-written as

$$dx = -\frac{1}{\gamma}(U'(x(t))dt - \sqrt{2\gamma T(x(t))}dW(t)), \tag{2.2.5}$$

where

$$dW(t) = \xi(t)dt \tag{2.2.6}$$

is the Wiener process.

The corresponding Fokker-Plank equation (FPE) to Itô stochastic differential equation (Itô SDE), given in Eq. (2.2.5) is given by [29]

$$\partial_t p(x,t) = \partial_x\{\frac{1}{\gamma}[U'(x)p(x,t) + \partial_x(T(x)p(x,t))]\}, \tag{2.2.7}$$

where $p(x,t)$ is the probability density of finding the Brownian particle at position x at time t. Equation (2.2.7) takes a simple form

$$\partial_t p(x,t) = -\partial_x J_0(x,t), \tag{2.2.8}$$

where

$$J_0(x,t) = \frac{-1}{\gamma}[U'(x)p(x,t) + \partial_x(T(x)p(x,t))] \tag{2.2.9}$$

is the probability current density. The steady state solution $p_{ss}(x)$ of Eq. (2.2.8)

$$\partial_t p_{ss}(x) = 0 \tag{2.2.10}$$

leads to a constant probability current density J_0 such that

$$U'(x)p_{ss}(x) + \frac{d}{dx}(T(x)p_{ss}(x)) = -\gamma J_0. \tag{2.2.11}$$

Using the particular potential and temperature profiles of the model defined by Eqs. (2.1.1) and (2.1.2) in Eq. (2.2.11) we get the relations

$$\frac{dp_{ss}(x)}{dx} + \frac{U_o}{L_1 T_h}p_{ss}(x) = -\frac{J_0\gamma}{T_h}, for - L_1 < x \leq 0 \tag{2.2.12}$$

and

$$\frac{dp_{ss}(x)}{dx} - \frac{U_o}{L_2T_c}p_{ss}(x) = -\frac{J_0\gamma}{T_c}, for 0 < x \leq L_2. \tag{2.2.13}$$

Equations (2.2.12) and (2.2.13) are easily solvable by the method of variation of parameters. The corresponding homogenous equation to Eq. (2.2.12) is given by

$$\frac{dp_{ss}(x)}{dx} + \frac{U_o}{L_1T_h}p_{ss}(x) = 0, \tag{2.2.14}$$

whose solution, say $p_{ssh}(x)$, is immediate. i.e.,

$$p_{ssh}(x) = C\exp(\frac{-U_o}{L_1T_h}x), \tag{2.2.15}$$

where C is a constant. Then, by method of variation of parameters, the general solution to Eq. (2.2.12) is given by

$$p_{ss}(x) = V(x)\exp(-\frac{U_o}{L_1T_h}x). \tag{2.2.16}$$

Substituting Eq. (2.2.16) in Eq. (2.2.12), it follows that

$$V(x) = C - \frac{J_0\gamma L_1}{U_o}\exp(\frac{U_o}{L_1T_h}x). \tag{2.2.17}$$

Combination of Eqs. (2.2.16) and (2.2.17) gives

$$p_{ss}(x) = C\exp(\frac{-Uo}{L_1T_h}x) - \frac{J_0\gamma L_1}{Uo}. \tag{2.2.18}$$

Similarly, the general solution to Eq. (2.2.13) takes a simple form

$$p_{ss}(x) = \hat{C}\exp(\frac{Uo}{L_2T_c}x) + \frac{J_o\gamma L_2}{Uo}, \tag{2.2.19}$$

for some constant $\hat{C}$. Hence eqs. (2.2.18) and (2.2.19) give a steady state probability density for $-L_1 < x \leq 0$ and $0 < x \leq L_2$, respectively.

To eliminate the constants C and $\hat{C}$ and solve for J_0, the following conditions are used.

(i). Periodic boundary condition, i.e.,

$$p_{ss}(-L_1) = p_{ss}(L_2). \tag{2.2.20}$$

(ii). Continuity of the steady state probability density, $p_{ss}(x)$, at x=0, i.e.,

$$\lim_{x \to 0^+} p_{ss}(x) = \lim_{x \to 0^-} p_{ss}(x), \tag{2.2.21}$$

where "+" and "-" denote the limit approach from left and from right, respectively.

(iii). Normalization of the steady state probability density, $p_{ss}(x)$, over a period, i.e.,

$$\int_{-L_1}^{L_2} p_{ss}(x)dx = 1. \tag{2.2.22}$$

Using conditions i and ii into Eqs. (2.2.18) and (2.2.19), solving for C and $\hat{C}$, we obtain

$$C = \frac{J_0\gamma(L_1 + L_2)(1 - \exp(\frac{U_o}{T_c}))}{U_o(\exp(\frac{U_o}{T_h}) - \exp(\frac{U_o}{T_c}))}$$

and

$$\hat{C} = \frac{J_0\gamma(L_1 + L_2)(1 - \exp(\frac{U_o}{T_h}))}{U_o(\exp(\frac{U_o}{T_h}) - \exp(\frac{U_o}{T_c}))}. \tag{2.2.23}$$

Applying condition iii into Eqs. (2.2.18) and (2.2.19), together with the expressions for C and $\hat{C}$, we can solve for J_0 and show that

$$J_0 = \frac{U_o^2 B}{\gamma[U_o B(L_2^2 - L_1^2) - AD(L_1 + L_2)(L_1 T_h + L_2 T_c)]}, \tag{2.2.24}$$

where $A = (1 - \exp(\frac{U_o}{T_c}))$, $B = (\exp(\frac{U_o}{T_h}) - \exp(\frac{U_o}{T_c}))$, and $D = (1 - \exp(\frac{U_o}{T_h}))$. Equation (2.2.24) gives a constant unidirectional probability current density, J_0, which is directed towards positive x.

Now let's write Eq. (2.2.24) in terms of dimensionless units. Define

$$j_0 = \frac{\gamma L_2^2}{T_c} J_0 \tag{2.2.25}$$

so that j_0 is dimensionless. Introducing the dimensionless parameters

$$\mu = \frac{U_o}{T_c}, \lambda = \frac{L_2}{L_1}, \tau = \frac{T_h}{T_c} \tag{2.2.26}$$

and solving for j_0 in terms of these newly introduced parameters, after some algebra the current reduces to

$$j_0 = \frac{\lambda^2 \mu(\exp(\mu) - \exp(\mu/\tau))}{(\exp(\mu) - \exp(\mu/\tau))(\lambda^2 - 1) + \frac{(1-\exp(\mu))(1-\exp(\mu/\tau))(1+\lambda)(\tau+\lambda)}{\mu}}. \tag{2.2.27}$$

Equation (2.2.27) gives an expression for unidirectional probability current density $j_0 = j_0(\mu, \tau, \lambda)$ as a function of dimensionless model parameters μ, τ and λ. From Eq. (2.2.27) we see that at $\mu = 0$ (i.e., no barrier) j_0 is zero. Also, if $\tau = 1$ or $\lambda = 0$, the particle is in an isothermal bath so that j_0 is zero. However, for $\mu > 0, \tau > 1$ and $\lambda > 0$, there is particle current which flows towards the positive x direction. Thus, there is non-zero net particle current if and only if both the potential barrier and the temperature gradient exist. Now, let us look at how the probability current density j_0 characterized by the model parameters μ, τ and λ.

As one can see from Fig. 2.2 the current increases with μ ($\mu = \frac{U_o}{T_c}$) starting from zero for $\mu = 0$ till it attains its maximum value, say at μ_{jm}, then decays with $\mu > \mu_{jm}$ and goes to zero as μ goes to infinity when the other parameters are kept constant. At $\mu = 0$, i.e., no potential barrier, the particle is equally probable to go either to the right or to the left. As a result, there is no net current. But as one increases the potential barrier gradually, the particle is biased to move in the positive x direction. Because, when the particle is in the hot reservoir, it experiences higher

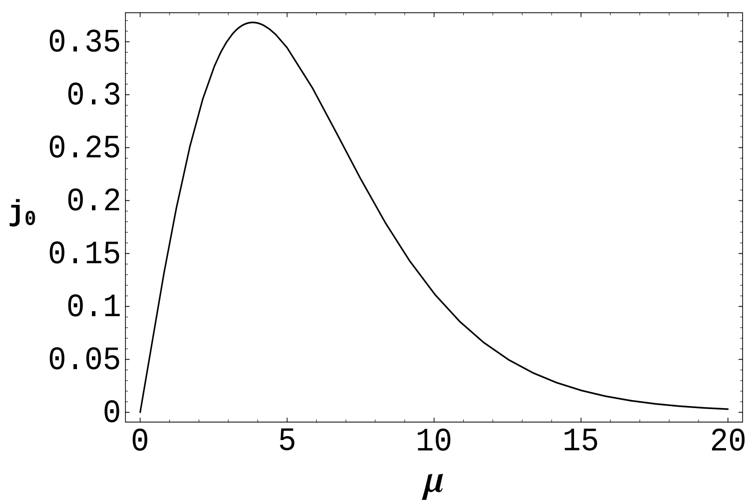

Figure 2.2: Plot of j_0 versus μ for $\lambda = 1$,$\tau = 2$.

thermal kick with more frequency than when it is in the cold reservoir. Hence, the particle is more energetic to climb up the hill when it is in the hot reservoir than when it is in the cold reservoir. In other words, the particle is more likely to move in the positive x direction than in the reverse way. Consequently, there is net particle current towards the right. For $\mu \leq \mu_{jm}$ the net particle current from hot reservoir to cold reservoir (in the positive x direction) increases with μ. Because for values of μ in the interval $(0, \mu_{jm}]$, a particle in the hot bath is energetic enough to climb up the hill and to overcome the impact of frictional force but for a particle in the cold bath it is difficult to climb up the hill (i.e., the probability of going to the negative

x direction decreases). As a result, the probability current density j_0 increases with μ. As μ is increased further (beyond μ_{jm}), the particle faces difficulty to climb up the hill even if it is in the hot bath. Therefore, the current starts falling with μ and finally goes to zero as μ tends to infinity.

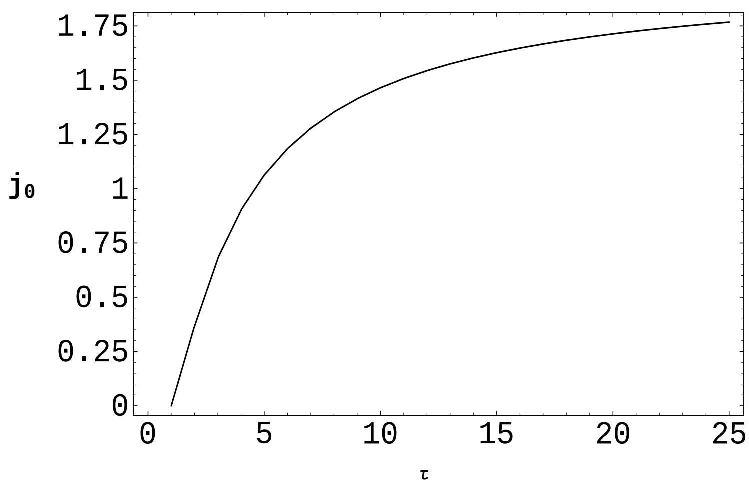

Figure 2.3: Plot of j_0 versus τ for $\lambda = 1$, $\mu = 4$.

Figure 2.3 shows how probability current density behaves with τ ($\tau = \frac{T_h}{T_c}$) when the other parameters are kept constant. At $\tau = 1$, i.e., when the medium is thermally in equilibrium, current is zero. As τ increases the particle experiences higher thermal kick with high frequency in the hot bath than in the cold bath so that there is net particle current from the hot bath to the cold bath (to the right) provided that $\mu > 0$

and $\lambda > 0$; otherwise net current is zero for $\mu = 0$ or $\lambda = 0$ for any value of τ. The plot shows that if one continues increasing τ, j_0 also continues increasing monotonously.

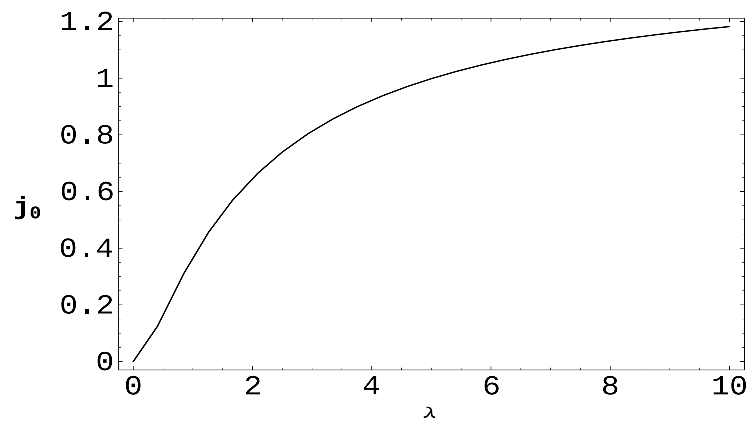

Figure 2.4: Plot of j_0 versus λ for $\tau = 2$, $\mu = 4$.

Plot of j_0 versus λ ($\lambda = \frac{L_2}{L_1}$) shows that probability current density increases with λ also monotonously. At $\lambda = 0$ (i.e., $L_2 = 0$) the Brownian particle remains in a isothermal bat (hot bath) so that no net particle current ($j_0 = 0$). But, for $\lambda > 0$ there is temperature gradient and hence non-zero particle current. As we keep increasing λ which is equivalent to decreasing L_1 and increasing L_2 (assuming $L = L_1 + L_2$ is constant), the mean first passage time from the hot bath of width L_1 to the cold bath of width L_2 decreases. In other words, rate of transition, which is the inverse of the mean passage time, from the hot bath to the cold bath increases. As a result j_0 increases with λ monotonously as shown in Fig. 2.4.

2.3 Stochastic Energetics

One of the most important issues in the study of microscopic heat engine is their energetics such as the power consumption of the machine, efficiency of energy conversion of the machine and so on.

In this section we will find expressions for the energy extracted by the Brownian particle from the hot reservoir Q_{h0}, work done by the engine W_0 and its efficiency η_0 per cycle in terms of the parameters introduced in the previous section.

As the particle moves from hot reservoir of width L_1 to cold reservoir of width L_2, it undergoes one cyclic motion. To find analytic expressions for quantities mentioned above, we start from Eq. (2.2.5). The equivalent Stratonovich stochastic differential equation to the Itô stochastic differential equation (2.2.5), for constant γ, is

$$dx = \frac{1}{\gamma}[(-U'(x) - \frac{1}{2}T'(x))dt + \sqrt{2\gamma T(x)}dW(t)]. \tag{2.3.1}$$

This can be written as

$$\sqrt{2\gamma T(x)}\xi(t) = \gamma\frac{dx}{dt} + \frac{dU(x)}{dx} + \frac{1}{2}\frac{dT(x)}{dx}. \tag{2.3.2}$$

The term in the LHS of Eq. (2.3.2) is the thermal force that a Brownian particle experiences. While in the hot reservoir, the particle gains energy from it. Part of this energy is used to climb up the barrier as the particle moves from $x = -L_1$ to $x = 0$ and to do work gainst the frictional force of the medium in going from $x = -L_1$ to $x = L_2$. The remaining part of the energy gained from the hot reservoir is leaked into the cold reservoir as the particle crosses the interface between the two regions. The particle gains energy only when it is in the hot reservoir so that the total energy extracted by the Brownian particle from the hot bath per cycle is

$$Q_{h0} = \lim_{\epsilon \longrightarrow 0}\int_{-(L_1+\epsilon)}^{0-\epsilon} \sqrt{2\gamma T(x)}\xi(t)dx. \tag{2.3.3}$$

Using Eqs. (2.3.2) and (2.3.3), we have

$$Q_{h0} = \lim_{\epsilon \longrightarrow 0} \int_{-(L_1+\epsilon)}^{0-\epsilon} (\gamma \frac{dx}{dt} + \frac{dU(x)}{dx} + \frac{1}{2}\frac{dT(x)}{dx})dx. \tag{2.3.4}$$

Which gives (where ϵ is positive)

$$Q_{h0} = \gamma v L_1 + U_o + \frac{1}{2}(T_h - T_c), \tag{2.3.5}$$

where v is mean drift velocity.

Consider the last term in RHS of Eq. (2.3.5): it is the amount of energy that the Brownian particle leaks into the cold bath as it crosses the interface between the two baths. Therefore, Eq. (2.3.5) gives the gross energy extracted from the hot reservoir by the Brownian particle.

The mean drift velocity is

$$v = \int_{-L_1}^{L_2} \frac{dx}{dt} p_{ss}(x)dx. \tag{2.3.6}$$

From Eq. (2.3.2)

$$\frac{dx}{dt} = \frac{1}{\gamma}[-\frac{dU(x)}{dx} - \frac{1}{2}\frac{dT(x)}{dx} + \sqrt{2\gamma T(x)}\xi(t)]. \tag{2.3.7}$$

We can combine equations (2.2.3), (2.2.12), (2.3.6) and (2.3.7) to get

$$v = J_0(L_1 + L_2). \tag{2.3.8}$$

Thus, Eq. (2.3.5) becomes

$$Q_{h0} = \gamma L_1(L_1 + L_2)J_0 + U_o + \frac{1}{2}(T_h - T_c). \tag{2.3.9}$$

The hot reservoir exerts a force of $\sqrt{2\gamma T(x)}\xi(t)$ on the Brownian particle as mentioned earlier in this section. Therefore, the work done W_0 by the engine per cycle can be obtained using the relation given by Eq. (2.3.2)as

$$W_0 = \int_{-L_1}^{L_2} \sqrt{2\gamma T(x)}\xi(t)dx$$

and

$$W_0 = \int_{-L_1}^{L_2} (\gamma \frac{dx}{dt} + \frac{dU(x)}{dx} + \frac{1}{2}\frac{dT(x)}{dx}) dx. \tag{2.3.10}$$

Since U(x) and T(x) are periodic, U(-L_1) = U(L_2) and T(-L_1) = T(L_2), the last two terms in the RHS of Eq. (2.3.10) vanish. Therefore, we get

$$W_0 = \int_{-L_1}^{L_2} (\gamma \frac{dx}{dt}) dx$$

and

$$W_0 = \gamma v (L_1 + L_2). \tag{2.3.11}$$

Using the value of v given in Eq. (2.3.8), W_0 becomes

$$W_0 = \gamma J_0 (L_1 + L_2)^2. \tag{2.3.12}$$

Next we explore the average power P_0: the rate at which the engine does work per cycle and see its dependency on the dimensionless parameters μ, τ and λ. The average power output per cycle P_0 is given by

$$P_0 = \int_{-L_1}^{L_2} \frac{dW_0}{dt} P_{ss}(x) dx. \tag{2.3.13}$$

Equations (2.2.3), (2.2.11) and (2.3.2) together with Eq. (2.3.13) gives

$$P_0 = W_0 J_0, \tag{2.3.14}$$

where J_0 and W_0 are given by equations (2.2.25) and (2.3.12), respectively. After some algebraic manipulations, in terms of dimensionless units power output becomes

$$P_0 = \frac{\lambda^2 \mu^4 (\exp(\mu) - \exp(\mu/\tau))^2}{[(\lambda + \tau)(1 - \exp(\mu)) + \mu \exp(\mu)(\lambda - 1) + \exp(\mu/\tau)(\exp(\mu)(\lambda + \tau) + \mu - \tau - \lambda(1 + \mu))]^2} \tag{2.3.15}$$

and for symmetric ratchet, i.e., $\lambda = 1$ it simplifies to

$$p_0 = \frac{\mu^4[\coth(\frac{\mu}{2}) - \coth(\frac{\mu}{2\tau})]^2}{4(1+\tau)^2}. \tag{2.3.16}$$

Therefore, $\mathrm{p}_0 = \mathrm{p}_0(\mu, \lambda, \tau)$ and $\mathrm{p}_0 = \mathrm{p}_0(\mu, \tau)$ given by Eqs. (2.3.15) and (2.3.16) are power output of the engine as a function of model parameters for asymmetric and symmetric ratchets respectively. The behavior of power output with respect to each of the parameters μ, λ and τ is discussed below.

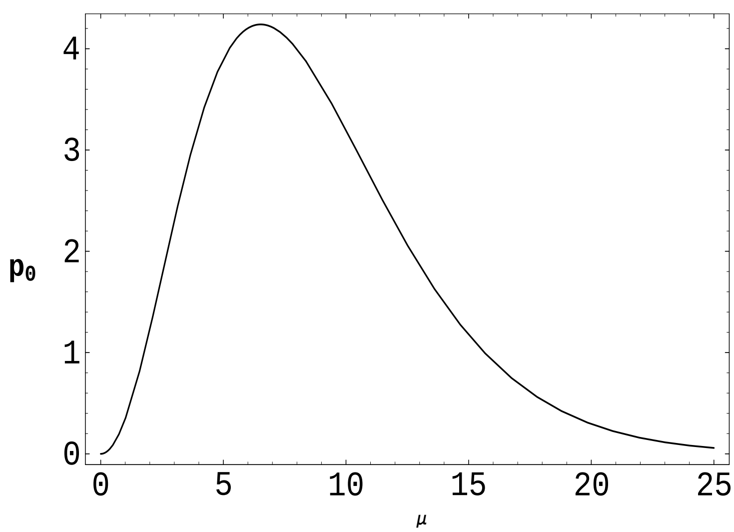

Figure 2.5: Plot of P_0 versus μ for $\lambda = 1$, $\tau = 4$.

Figure 2.5 shows plot of P_0 versus μ for $\tau = 4$ and $\lambda = 1$. As it can be seen form the figure, P_0 increases with μ starting form zero where μ itself is zero and attains its maximum value, say at μ_{mp0}. Then, starts decreasing with $\mu > \mu_{mp0}$ and finally becomes zero as μ tends to infinity. In section 2.2 we have seen that at $\mu = 0$ and as $\mu \longrightarrow \infty$ no net particle current so that power output is also zero in both cases. But increasing μ above zero results in directed particle current with some power output. Thus, there is maximum power output between the two extremes ($\mu = 0$ and $\mu \longrightarrow \infty$).

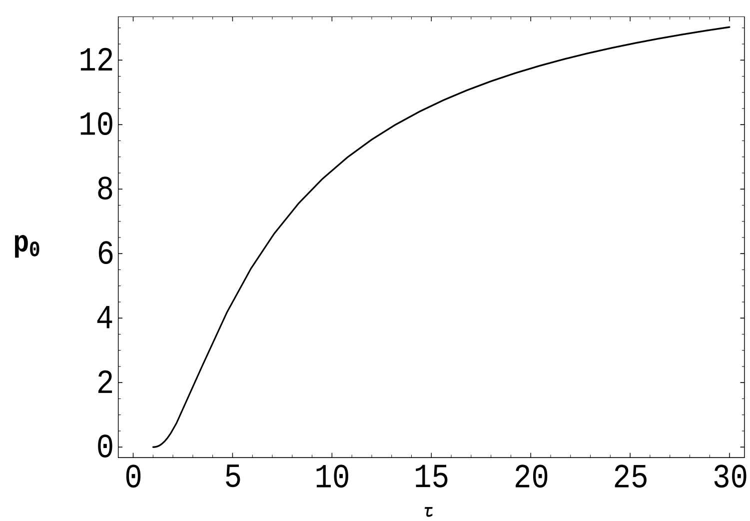

Figure 2.6: Plot of P_0 versus τ for $\lambda = 1$, $\mu = 4$.

Plot of P_0 versus τ is shown in Fig. 2.6. Average power monotonously increases with increase in τ when the other parameters are kept constant. At $\tau = 1$ the Brownian particle is in an isothermal bath (no temperature gradient). As a result there is no net particle current (also, for $\tau = 1$ Eq. (2.3.16) gives $\mathrm{P}_0 = 0$). If there is temperature gradient ($\tau > 1$), directed particle current is induced which increases with temperature gradient and so is the power output. We have shown in Fig 2.4

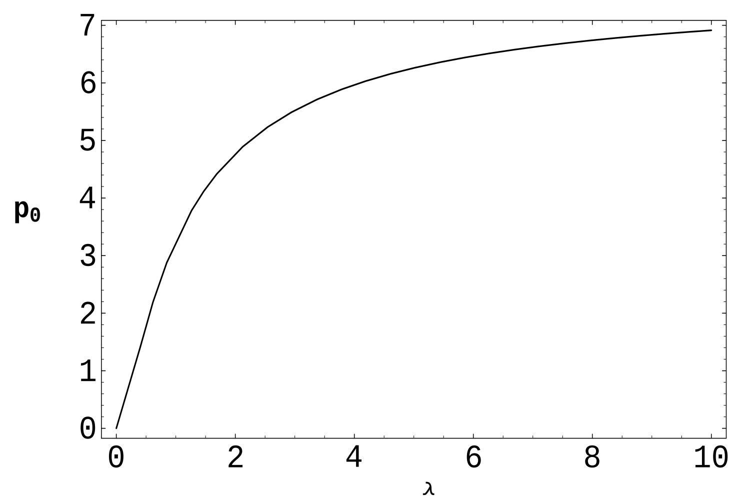

Figure 2.7: Plot of P_0 versus λ for $\mu = 4$, $\tau = 4$.

that probability current density increases with increase in λ for constant μ and τ. Due to this, power output of the engine also increases as λ increases monotonically.

Since all engines operate, necessarily, at loss [30], it is essential to study their efficiency. Next the efficiency η_0 of our engine: the ratio of the available work to the heat delivered by the hot reservoir is investigated in terms of the control parameters used in the modeling. Thus, we can define efficiency as

$$\eta_0 = \frac{W_0}{Q_{h0}}.$$

Using Eqs. (2.3.10) and (2.3.11), the expression for efficiency becomes

$$\eta_0 = \frac{\gamma J_0 (L_1 + L_2)^2}{\gamma L_1 (L_1 + L_2) J_0 + U_o + \frac{1}{2}(T_h - T_c)}. \tag{2.3.17}$$

After some algebra, in terms of dimensionless unit, efficiency simplifies to

$$\eta_0 = \frac{F_1}{F_2 F_3}, \tag{2.3.18}$$

where

$$F_1 = \mu(1+\lambda)(\exp(\mu) - \exp(\mu/\tau)),$$

$$F_2 = (\lambda - 1)(\exp(\mu) - \exp(\mu/\tau)) + \tfrac{(\lambda+\tau)(1-\exp(\mu))(1-\exp(\mu/\tau))}{\mu}$$

and

$$F_3 = \tfrac{1}{2}(\tau - 1) + \mu + \tfrac{\mu(\exp(\mu)-\exp(\mu/\tau))}{(\exp(\mu)-\exp(\mu/\tau))(\lambda-1)+\frac{(\lambda+\tau)(1-\exp(\mu))(1-\exp(\mu/\tau))}{\mu}}.$$

For $\lambda = 1$ (symmetric potential) the expression for efficiency takes a simple form:

$$\eta_0 = \frac{4\mu^2(\exp(\mu) - \exp(\mu/\tau))}{(1-\exp(\mu))(1-\exp(\mu/\tau))(\tau^2 + 2\mu + 2\mu\tau - 1 + \mu^2(\coth(\frac{\mu}{2\tau}) - \coth(\frac{\mu}{2})))}. \tag{2.3.19}$$

Equations (2.3.18) and (2.3.19) give an expression for efficiency as a function of model parameters for asymmetric and symmetric potential, respectively. Next we discuss how efficiency behaves with respect to the parameters μ, τ and λ.

Figure 2.8 shows efficiency as a function of temperature ratio τ. The upper curve corresponds to the case when the thermal leakage is ignored while the lower curve corresponds the case when thermal leakage is taken into account. In the first case, efficiency increases with τ monotonously. This is because, as the temperature of

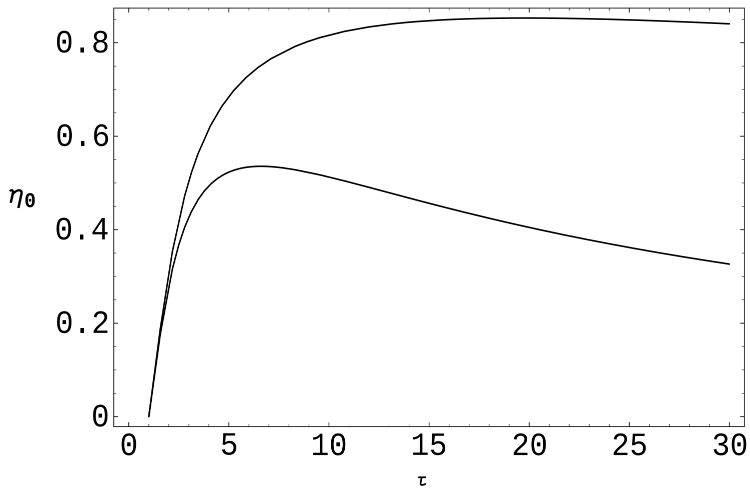

Figure 2.8: Plot of η_0 versus τ for λ= 1, μ = 4.

hot reservoir becomes higher relative to that of the cold one, the Brownian particle experiences strong thermal kick in the hot reservoir so that there is more particle current from hot to cold reservoir (to the right), i.e., more work is done by the engine. Hence there is an increase in the efficiency with τ. In the second case (thermal leakage taken into account), efficiency increases with increase in τ till it attains its maximum value at some value of τ. Then, starts falling for values of τ larger than some value. Because, for values of τ larger than some value, more energy goes to thermal leakage (more wastage of energy) and causes decrease in the efficiency of the engine.

On the other hand, keeping τ and λ unchanged, with τ greater than unity and λ

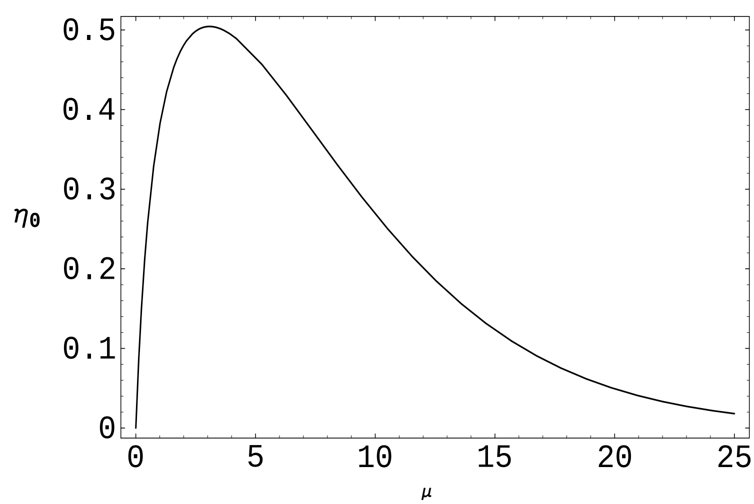

Figure 2.9: Plot of η_0 versus μ for $\lambda = 1$, $\tau = 4$.

> 0 necessarily, if there is no potential barrier, Brownian particle is equally likely to flow to either to the right or to left in Fig. 2.1. Hence, no net work is done by the engine so that efficiency is zero in this case. For large values of barrier height, say $\mu \longrightarrow \infty$, thermal noise intensity is not strong enough to cause the Brownian particle climb up such a barrier. Consequently, no particle flow even from locally hot region to that of cold region (to the right). So, efficiency is zero in this case also. But, if the potential barrier is increased slightly above zero, a particle in the hot reservoir is more energetic to cross the barrier than a particle in the cold reservoir because of its higher thermal intensity level in the hot the reservoir. Because of this, there is directed particle transport from hot to cold reservoir (to the positive x direction) and we get non-zero efficiency. Therefore, efficiency must have maxima between the two extremes of μ ($\mu = 0$ and $\mu \longrightarrow \infty$) at some value of $\mu = \mu_{m\eta 0}$ which depends on the values of τ and λ. Typical plot of η_0 versus μ is shown in Fig. 2.9.

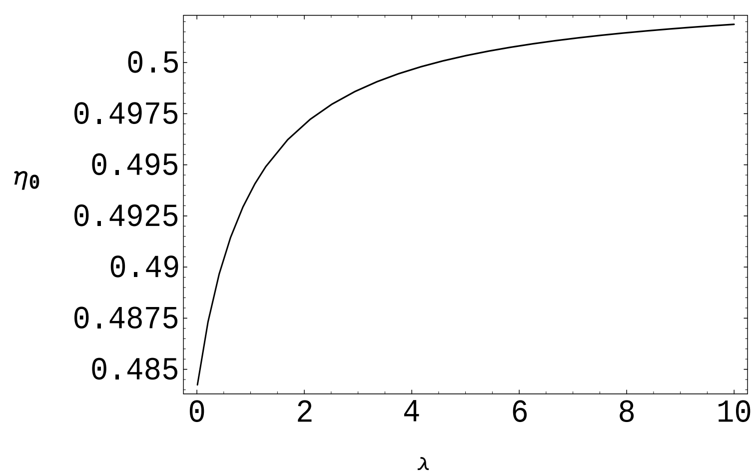

Figure 2.10: Plot of η_0 versus λ for $\mu = 4$, $\tau = 4$.

Plot of η_0 versus λ is shown in Fig. 2.10. Due to increasing of probability current density with increasing in λ (Fig. 2.4), efficiency of the engine increases as λ increases.

2.4 Maximum Power and Maximum Efficiency Regimes

In the previous section it was shown that both power output and efficiency attain their maximum values at some value of μ (μ_{mp0} and $\mu_{m\eta 0}$, respectively), which are functions of λ and τ. In this section maximum power output points μ_{mp0} and maximum efficiency points $\mu_{m\eta 0}$ as well as maximum power output (p_{mp0}), efficiency at maximum power output η_{mp0}, maximum efficiency $\eta_{m\eta 0}$ and power output at maximum efficiency $p_{m\eta 0}$ are obtained numerically as a function of τ for $\lambda = 1$, where $p_{mp0} = p(\mu_{mp0})$, $\eta_{mp0} = \eta(\mu_{mp0})$, $\eta_{m\eta 0} = \eta(\mu_{m\eta 0})$ and $p_{m\eta 0} = p(\mu_{m\eta 0})$.

To obtain maximum power output points μ_{mp0}, Eq. (2.3.16) is used together with the condition

$$\frac{\partial p_0}{\partial \mu}\Big|_{\mu=\mu_{mp0}} = 0, \tag{2.4.1}$$

which gives

$$\tau(2e^{\mu}-2e^{2\mu}+2e^{\mu(2+\frac{1}{\tau})}+e^{\frac{2\mu}{\tau}}(2+e^{\mu}(\mu-2)))+\mu(\tau e^{\mu}-e^{\mu(2+\frac{1}{\tau})})-e^{\frac{\mu}{\tau}}(2\tau+\mu+2e^{\mu}(\tau-1)\mu) = 0, \tag{2.4.2}$$

where $\mu = \mu_{mp0}$.

Equation (2.4.2) is solvable numerically only. So, solving it numerically, we obtain solutions μ_{mp0} for various values of τ keeping λ constant. Figure 2.11 shows plot of μ_{mp0} versus τ which is obtained by evaluating Eq. (2.4.2) numerically for $\lambda = 1$. In solving Eq. (2.4.2) numerically, initially τ is set to be equal to 1.1 with a time step 5×10^{-3} and the corresponding solution μ_{mp0} is obtained with an accuracy of 10^{-6}. Plot of μ_{mp0} versus τ shows μ_{mp0} increase with τ almost linearly.

For maximum efficiency points the condition

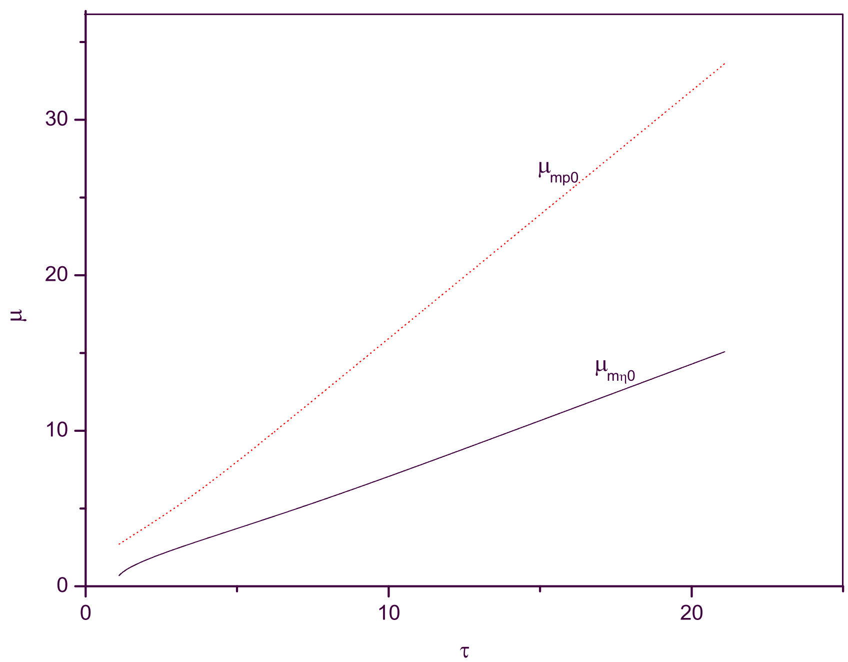

Figure 2.11: Plot of μ_{mp0} and $\mu_{m\eta0}$ versus τ.

$$\frac{\partial \eta_0}{\partial \mu}\Big|_{\mu=\mu_{m\eta 0}} = 0, \tag{2.4.3}$$

should hold. Using the above condition in Eq. (2.3.19), the equation given in appendix A (Eq. A.0.1) is obtained. Its solution is maximum efficiency point $\mu_{m\eta0}$, the point at which efficiency attains its maximum value.

Numerical solution $\mu_{m\eta0}$ of Eq. (2.3.19) versus τ is plotted in Fig. 2.11 for the same value of λ, initial value of τ, time step and accuracy used in evaluating maximum power output points μ_{mp0}. Similar to μ_{mp0} , $\mu_{m\eta0}$ increases with τ linearly but with different slope. Figure 2.11 shows that the slope for μ_{mp0} versus τ is greater than that of $\mu_{m\eta0}$ versus τ for the same value of λ, i.e, μ_{mp0} and $\mu_{m\eta0}$ increase at different rate for the same increase in τ. In short, $(\mu_{mp0}, \tau) > (\mu_{m\eta0}\ , \tau)$. The region between curves μ_{mp0} and $\mu_{m\eta0}$ in Fig 2.11 (i.e., the region between maximum power points and maximum efficiency points) corresponds to the operating region of real heat engine [28] and references therein.

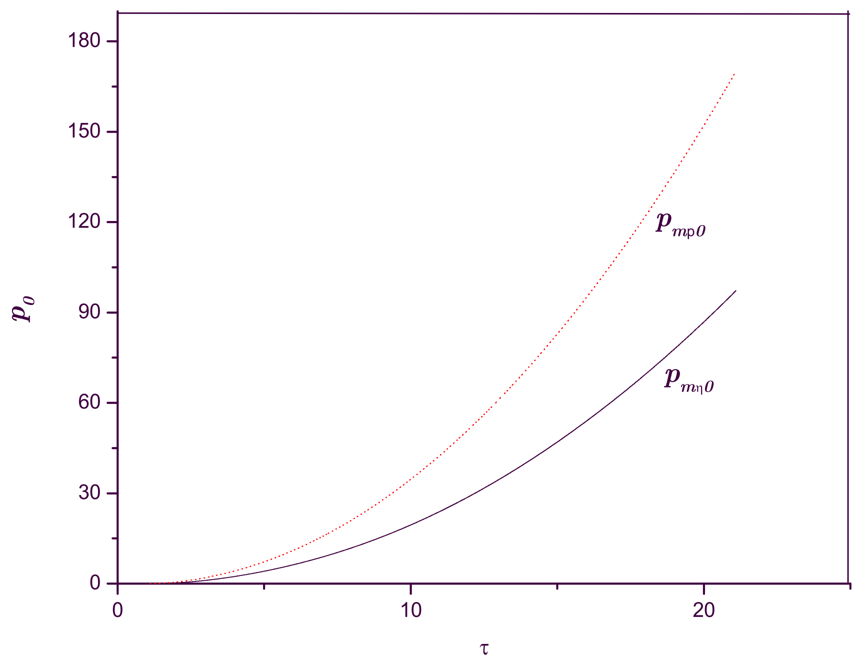

Figure 2.12: Plot of P_{mp0} and $P_{m\eta0}$ versus τ.

Now, substituting numerical solution of Eq. (2.4.2) and Eq. (A.0.1) in appendix A into Eq. (2.3.16), maximum power output, $p_{mp0} = p(\mu_{mp0})$, and the power output at the maximum efficiency regime, $p_{m\eta0} = p(\mu_{m\eta0})$, are obtained. Figure 2.12 shows the plot of p_{mp0} and $p_{m\eta0}$ versus τ for $\tau > 1$ and $\lambda = 1$. From the plot both p_{mp0} and

$p_{m\eta 0}$ increase monotonically with τ and $p_{mp0} \geq p_{m\eta 0}$.

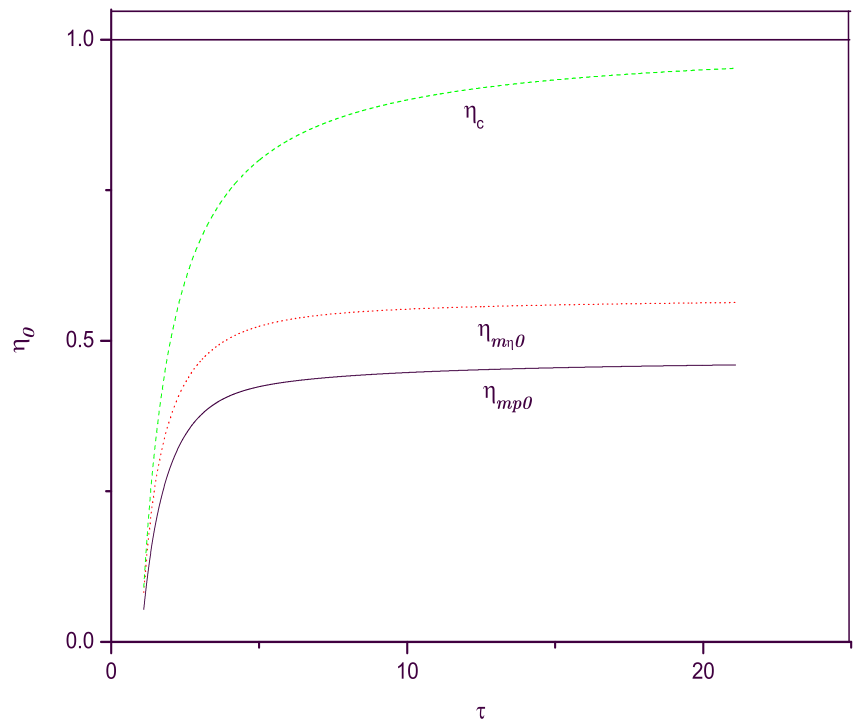

Figure 2.13: Plot of η_{mp0}, $\eta_{m\eta 0}$ and η_c versus τ.

Before concluding this section, the maximum efficiency and efficiency at the maximum power are discussed. Once again, using numerical solutions of Eq. (2.4.2) and Eq. (A.0.1) of appendix A in to Eq. (2.3.19) , maximum efficiency $\eta_{m\eta 0} = \eta(\mu_{m\eta 0})$ and efficiency at maximum power regime $\eta_{mp0} = \eta(\mu_{m\eta 0})$ are obtained. Plot of $\eta_{m\eta 0}, \eta_{mp0}$ and η_c versus τ are shown in Fig. 2.13 for $\lambda = 1$, where η_c is Carnot's efficiency. From the plot one can see that $\eta_{m\eta 0}$ and η_{mp0} increase with τ monotonously and $\eta_{m\eta 0} \geq \eta_{mp0}$.

Due to the the ever existing thermal leakage discussed in section (2.3), the efficiency of our engine always less than that of Carnot's efficiency, i.e., $\eta_{m\eta 0} < \eta_c$. Here also, the region between curves $\eta_{m\eta 0}$ and η_{mp0} in Figs. 2.12 and 2.13 are the operating regions of real heat engine.

Chapter 3

A Brownian Particle in Tilted Ratchet-Potential Far from Thermal Equilibrium with Load

In the previous Chapter we developed stochastic model for a microscopic heat engine or Brownian motor using a Brownian particle moving through a highly viscous medium, in an alternately placed hot and cold heat baths, in a periodic asymmetric saw-tooth potential where there is no external load.

In this Chapter, we study the generalization of the stochastic model developed in the previous chapter in the presence of static external force. For this generalized model, the expressions for the probability current density and its energetics will be found and discussed in terms of the parameters introduced in chapter two in addition to the new parameter, load, and compared with the previous results obtained in Chapter two. Then, we will study power and efficiency at maximum power regimes and at maximum efficiency regimes numerically and conclude the Chapter.

3.1 Steady State Solution and Probability Current Density

In this section steady state solution to our generalized model and an expression for probability current density for the steady state system in terms of the parameters used in the modeling technique will be obtained.

As we presented in section 2.1, we start by considering a Brownian particle moving in a highly viscous medium and one-dimensional asymmetric periodic saw-tooth potential of barrier height U_o, in an alternately placed hot and cold heat baths, in the presence of static external force (f) so that the potential corresponding to the external force is linear (fx). A single period saw-tooth potential, $U(x)$, located in the vicinity of $x = 0$ which the Brownian particle experiences is given by

$$U(x) = \begin{cases} (f + \frac{U_o}{L_1})x + U_o & \text{for } -L_1 < x \leq 0 \\ (f - \frac{U_o}{L_2})x + U_o & \text{for } 0 < x \leq L_2, \end{cases} \tag{3.1.1}$$

with the same temperature profile given in section 2.2, Eq.(2.1.2).

Figure 3.1 shows plot of periodic asymmetric saw-tooth potential in the presence of static external force with its temperature profile. The potential is tilted due to the external load. The hot reservoir has width of L_1 and the cold reservoir of width L_2 as before. The potential as well as the temperature are periodic with same period $L = L_1 + L_2$. The motion of a Brownian particle in such a tilted ratchet-potential can be described by stochastic dynamics as

$$m\ddot{x}(t) = -U'(x(t)) - \gamma\dot{x}(t) + \sqrt{2\gamma k_B T(x)}\xi(t), \tag{3.1.2}$$

where $m, x(t)$, γ, k_B, T(x), and $\xi(t)$ are as defined in section 2.1 and $\xi(t)$ satisfies Eqs. (2.2.3) and (2.2.4). For the over damped motion, the inertial term $m\ddot{x}(t)$, is

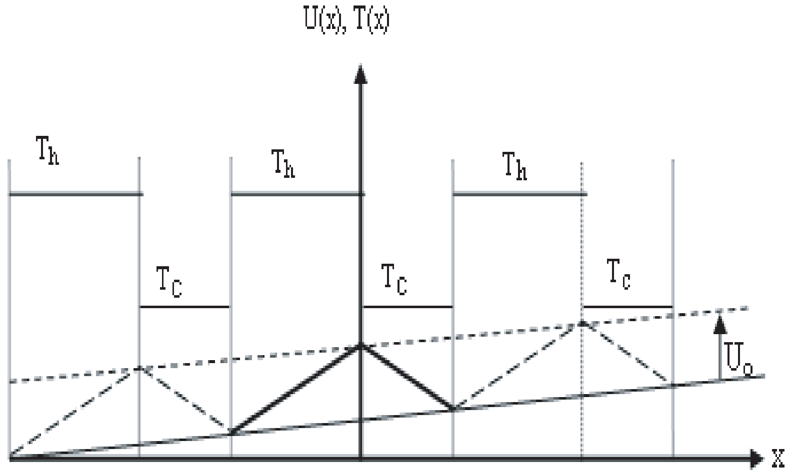

Figure 3.1: Plot of periodic asymmetric saw-tooth potential in the presence of static external force, $U(x)$, and its temperature profile.

negligible so that the dynamics in Eq. (3.1.2) reduces to a stochastic differential equation (SDE)

$$dx(t) = \frac{-1}{\gamma}(\frac{dU(x)}{dx} - \sqrt{2\gamma T(x)}dW(t)), \tag{3.1.3}$$

where k_B is taken to be unity and $dW(t)$ is the Wiener process introduced in Chapter 2. Equation (3.1.3) is also equivalent to the following Fokker-Plank equation (FPE)

$$\partial_t p(x,t) = \frac{1}{\gamma}\partial_x(\frac{dU(x)}{dx}p(x,t) + \partial_x(T(x)p(x,t))). \tag{3.1.4}$$

The above Fokker-Plank equation (Eq. 3.1.4) can be written as

$$\partial_t p(x,t) = -\partial_x J(x,t), \tag{3.1.5}$$

where

$$J(x,t) = \frac{-1}{\gamma}(\frac{dU(x)}{dx}p(x,t) + \partial_x(T(x)p(x,t))) \tag{3.1.6}$$

is the probability current density in the presence of static external force and $p(x,t)$ is the same as defined in the previous chapter. For steady state case, $\partial_t p(x,t) = 0$, i.e., the probability density is independent of time so that $p(x,t) = p_{ss}$(x), for any time t. From Eq. (3.1.5) this implies that at steady state, probability current density is constant in both time and space arises

$$J(x,t) = J. \tag{3.1.7}$$

Therefore, combination of Eqs. (3.1.1), (3.1.6) and (3.1.7) gives

$$\frac{dp_{ss}(x)}{dx} + \frac{1}{T_h}(f + \frac{U_o}{L_1})p_{ss}(x) = \frac{-J\gamma}{T_h}, if - L_1 < x \leq 0 \tag{3.1.8}$$

and

$$\frac{dp_{ss}(x)}{dx} + \frac{1}{T_c}(f - \frac{U_o}{L_2})p_{ss}(x) = \frac{-J\gamma}{T_c}, if 0 < x \leq L_2. \tag{3.1.9}$$

Starting with Eq. (3.1.8), its homogenous solution, $p_{ssh}(x)$, is given by

$$p_{ssh}(x) = C_1 \exp(-\alpha x), \tag{3.1.10}$$

where C_1 is a constant and $\alpha = \frac{1}{T_h}(f + \frac{U_o}{L_1})$. Therefore, the general solution to Eq. (3.1.8) using the method of variation of parameters can be obtained as

$$p_{ss}(x) = g(x)\exp(-\alpha x). \tag{3.1.11}$$

Substituting Eq. (3.1.11) in Eq. (3.1.8), we get

$$g(x) = C_1 - \frac{J\gamma}{\alpha T_h}\exp(\alpha x), \tag{3.1.12}$$

such that

$$p_{ss}(x) = C_1 \exp(-\alpha x) - \frac{J\gamma}{\alpha T_h}. \tag{3.1.13}$$

Similarly, for Eq. (3.1.9), we find

$$p_{ss}(x) = C_2 \exp(-\beta x) - \frac{J\gamma}{\beta T_c}, \tag{3.1.14}$$

where C_2 is a constant and $\beta = \frac{1}{T_c}(f - \frac{U_o}{L_2})$. Using conditions i and ii given in section 2.2 (Eqs. 2.2.20 and 2.2.21) into Eqs. (3.1.13) and (3.1.14), then, solving for C_1 and C_2, we obtain

$$C_1 = J\gamma(\frac{1}{\alpha T_h} - \frac{1}{\beta T_c})(\frac{1 - \exp(-\beta L_2)}{\exp(\alpha L_1) - \exp(-\beta L_2)}) \tag{3.1.15}$$

and

$$C_2 = J\gamma(\frac{1}{\alpha T_h} - \frac{1}{\beta T_c})(\frac{1 - \exp(-\alpha L_1)}{\exp(\alpha L_1) - \exp(-\beta L_2)}). \tag{3.1.16}$$

The normalization condition iii of section 2.2 gives us

$$\frac{C_2}{\beta}(1 - \exp(-\beta L_2)) + \frac{C_1}{\alpha}(1 - \exp(\alpha L_1)) - J\gamma(\frac{L_2}{\beta T_c} + \frac{L_1}{\alpha T_h}) = 1. \tag{3.1.17}$$

Substituting the values of C_1 and C_2 given in Eqs. (3.1.15) and (3.1.16) into Eq. (3.1.17) and solving for J, we get

$$J = \frac{\alpha\beta T_h T_c f_1}{\gamma(f_2 - f_3)}, \tag{3.1.18}$$

where

$f_1 = \exp(\alpha L_1) - \exp(-\beta L_2)$,

$f_2 = (\frac{1}{\beta} - \frac{1}{\alpha})(\beta T_c - \alpha T_h)(1 - \exp(\alpha L_1))(1 - \exp(-\beta L_2))$,

and

$f_3 = (L_1 \beta T_c + L_2 \alpha T_h)(\exp(\alpha L_1) - \exp(-\beta L_2))$.

If J is multiplied by $\frac{\gamma L_1 L_2}{T_c}$, it becomes dimensionless. Therefore, the dimensionless probability current density j is given by

$$j = \frac{\alpha\beta L_1 L_2 T_h f_1}{f_2 - f_3}. \tag{3.1.19}$$

In addition to the dimensionless units introduced in section 2.2, we introduce one more dimensionless unit

$$\rho = \frac{L_1 f}{T_c}. \tag{3.1.20}$$

Re-substituting the values of α and β, in terms of the parameters μ, τ, λ and ρ, the expression for j takes a simple form:

$$j = \frac{g_1}{g_2 + g_3}, \tag{3.1.21}$$

where

$\mathrm{g}_1 = (\mu - \lambda\rho)(\mu + \rho)(\exp(\frac{\mu+\rho}{\tau}) - \exp(\mu - \lambda\rho))$,

$\mathrm{g}_2 = (\rho(1 + \lambda) + \mu(\lambda - \frac{1}{\lambda}))(\exp(\frac{\mu+\rho}{\tau}) - \exp(\mu - \lambda\rho))$

and

$\mathrm{g}_3 = \mu(1 + \lambda)(\frac{1}{\lambda\rho-\mu} - \frac{\tau}{\lambda(\mu+\rho)})(1 - \exp(\frac{\mu+\rho}{\tau}))(1 - \exp(\mu - \lambda\rho))$.

Thus, Eq. (3.1.22) gives an expression for a directed probability current density as a function of model parameters μ, τ, λ and ρ. Most of these parameters favor directed particle current from the hot bath to the cold bath (towards the positive x direction) till j attains its maximum value but ρ favors the flow of particle in the reverse direction. So, depending on the values of these parameters the probability current density could be positive, zero or negative. If j is positive (flows from the hot bath to the cold bath towards positive x direction), our model functions as an engine and as a refrigerator under the opposite condition. Therefore, the appropriate choice of the parameters μ, τ, λ and ρ determines the function of the model. Next, we analyze and discuss how j varies with changes in one of the model parameters.

Figure 3.2 shows plot of j as a function of μ ($\mu = \frac{U_o}{T_c}$) with the other parameters are kept constant. Both j_0 and j show similar behavior with respect to μ. In the

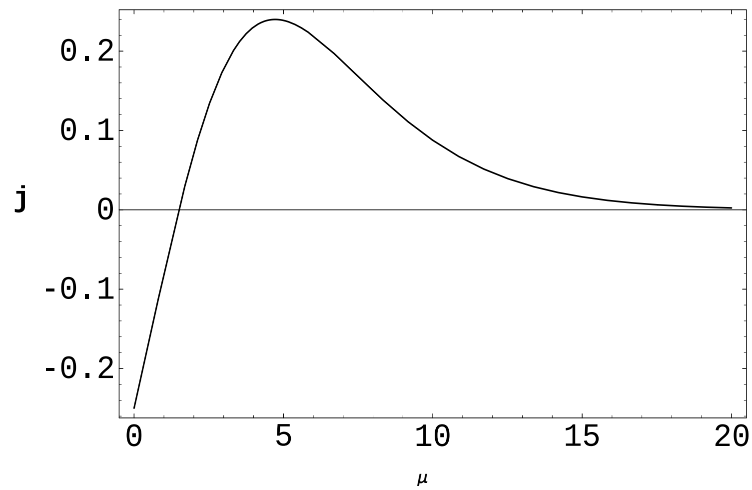

Figure 3.2: Plot of j versus μ for $\lambda = 1$, $\rho = 0.5$, $\tau = 2$

case of zero external load at $\mu = 0$, $j_0 = 0$. But in the presence of non-zero constant external load, at $\mu = 0$, $j < 0$ (negative) and increases with μ. At some value of μ, say μ_0, j becomes zero: as one keeps increasing μ above μ_0 j becomes positive and attains its maximum value at some other value (μ_{jm}). Then, decreases as μ increases for $\mu > \mu_{jm}$ and returns to zero as μ approaches infinity. The negative value of current for $\mu < \mu_0$ (i.e., the flow of current from cold reservoir to hot reservoir (to the left)) is due to the opposing external load which has higher effect than μ. At $\mu = \mu_0$ the current is zero because at this point the load (ρ) and the barrier height (μ_0) have the same but opposite effect on the flow of current. For values of $\mu > \mu_0$, the Brownian particle acquires enough energy from the hot reservoir which enables it to overcome the opposing effect of the external force and climb up the potential barrier so that there is net particle current from the hot reservoir to the cold reservoir (to the right), i.e., j is positive and the model is used as an engine in this region. For values of $\mu > \mu_{jm}$, the current decreases as μ increases. In this case thermal kicks acquired from the hot reservoir is not strong enough to make the particle cross the the potential barrier and overcome the opposing effect of the external load. So that the probability of going from the hot bath to the cold bath (to the right) decreases, hence decreasing in current with increasing μ. As one can see from comparing Figs. 2.2 and 3.2, for the same values of λ and τ, a decrease in maximum current can be achieved in the latter case due to the negative effect of the load (maximum probability current density $>$ 0.35 for the former case and $<$ 0.3 for the latter case: compare Figs. 2.2 and 3.2).

Figure 3.3 shows the plot of $\frac{j}{j_0}$ vs ρ ($\rho = \frac{fL_1}{T_c}$) for the other parameters fixed. The figure demonstrates that $\frac{j}{j_0}$ decreases as ρ increases almost linearly, starting from one where the external load is 0.

Figure 3.4 shows the property of j as a function of temperature ratio (τ) keeping the other parameters constant. For small values of τ, j is negative because at these values of τ the effect of external load which causes current to flow in the negative x direction (from cold bath to hot bath) dominates the effect of τ which favors the flow of current in the reverse direction. However, as the temperature gradient is increased further there will be net current towards the positive x direction. From the plot we can see that j increases with τ monotonously starting from some negative value. Comparing Fig. 2.3 and Fig. 3.4, for the same value of τ and λ, the maximum possible value of j is less than that of j_0 due to the negative impact of the external load.

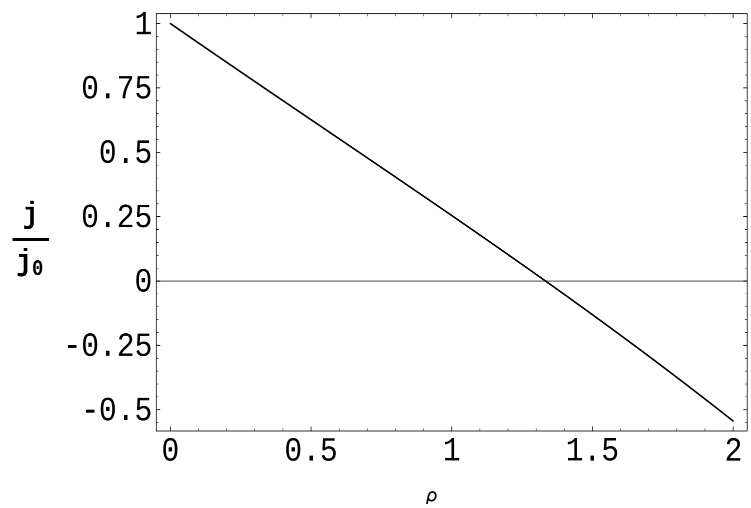

Figure 3.3: Plot of $\frac{j}{j_0}$ versus ρ for $\lambda = 1$, $\mu = 4$, $\tau = 2$

Figure 3.5 demonstrates the effect of the external load ρ on probability current density j. Here as shown in the figure, when the external load acts against current, j should decrease as ρ increases. The probability current density and the static external load have inverse linear relationship as shown in the plot.

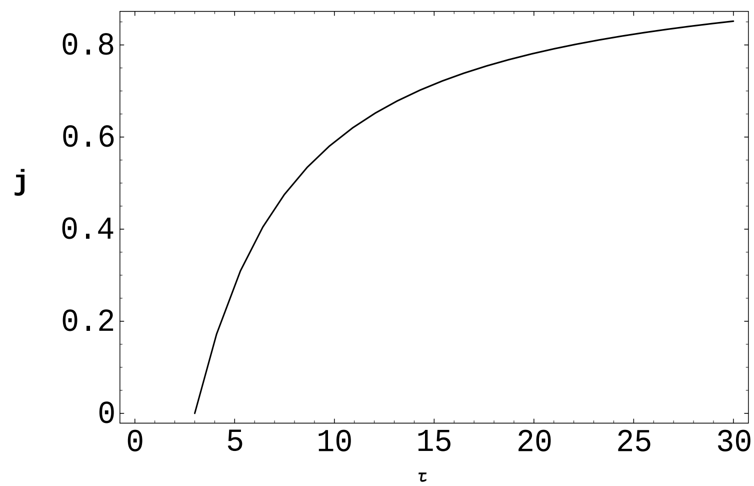

Figure 3.4: j versus τ for $\lambda = 1$, $\mu = 4$, $\rho = 2$

3.2 Stochastic Energetics with Non-zero Static External Load

In section 2.3 we emphasis that one of the important points to be addressed about microscopic heat engines is their energetics. In this section also we study the energetics of our generalized model in the presence of static external load ρ. Expressions for the energy transferred to the Brownian particle in the hot reservoir Q_h, work done by the engine W and its efficiency η per cycle are found and discussed.

The Stratonovich stochastic differential equation equivalent to the Itô stochastic

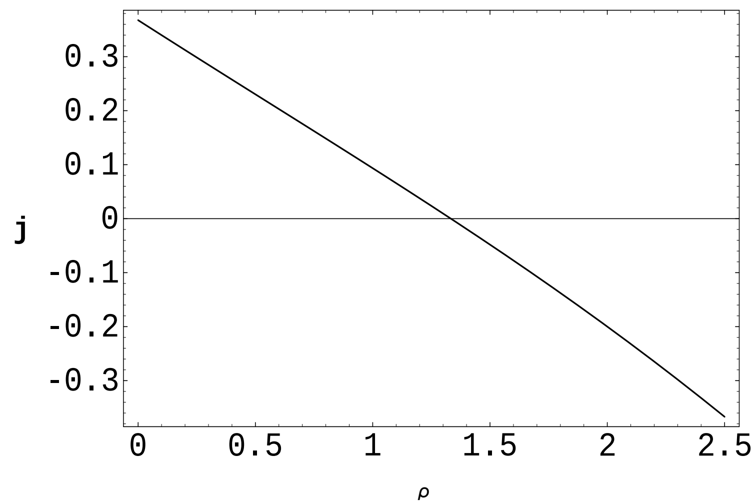

Figure 3.5: Plot of j versus ρ for $\lambda = 1$, $\mu = 4$, $\tau = 2$

differential equation given in Eq. (3.1.3) is given by

$$dx(t) = \frac{1}{\gamma}(\frac{-dU(x)}{dx} - \frac{1}{2}\frac{dT(x)}{dx})dt + \sqrt{2\gamma T(x)}dW(t)$$

or

$$\sqrt{2\gamma T(x)}\xi(t) = \gamma\frac{dx}{dt} + \frac{dU(x)}{dx} + \frac{1}{2}\frac{dT(x)}{dx}. \tag{3.2.1}$$

Following similar argument as in see section 2.3, Q_h determined from

$$Q_h = \lim_{\epsilon \longrightarrow 0}\int_{-(L_1+\epsilon)}^{0-\epsilon}\sqrt{2\gamma T(x)}\xi(t)dx$$

or

$$Q_h = \lim_{\epsilon \longrightarrow 0}[\int_{-(L_1+\epsilon)}^{0-\epsilon}\gamma(\frac{dx(t)}{dt})dx + \int_{-L_1}^{0+\epsilon}\frac{dU(x)}{dx}dx + \frac{1}{2}\int_{-L_1}^{0+\epsilon}\frac{dT(x)}{dx}dx], \tag{3.2.2}$$

which gives (where $\epsilon > 0$)

$$Q_h = \gamma v L_1 + U_o + f L_1 + \frac{1}{2}(T_h - T_c). \tag{3.2.3}$$

Using the expression for the drift velocity (v) given by Eq. (2.3.8), we get

$$Q_h = \gamma L_1 (L_1 + L_2) J + U_o + f L_1 + \frac{1}{2}(T_h - T_c). \tag{3.2.4}$$

Using the same method used in section 2.3, the work done by the engine per cycle is

$$W = (\gamma v + f)(L_1 + L_2). \tag{3.2.5}$$

However, from Eq. (2.3.8) the mean drift velocity is given

$$v = J(L_1 + L_2). \tag{3.2.6}$$

Thus, the work done becomes

$$W = \gamma J (L_1 + L_2)^2 + f(L_1 + L_2). \tag{3.2.7}$$

Dividing Eq. (3.2.7) by T_c gives the work done in terms of dimensionless quantities as

$$w = (1 + \lambda)(\rho + (1 + \frac{1}{\lambda})j), \tag{3.2.8}$$

where j is as given in Eq. (3.1.22).

The average power output per cycle is

$$P = WJ. \tag{3.2.9}$$

The dimensionless average power (as a function of dimensionless units) is given by

$$p = wj \tag{3.2.10}$$

By taking the values of j and w given in Eqs. (3.1.21) and (3.2.8) and putting in Eq. (3.2.10), the power output for symmetric potential (i.e., $\lambda = 1$) simplifies to

$$p = \frac{h_2^2(h_1 h_3 + 4)}{h_3^2}, \tag{3.2.11}$$

where

$\mathrm{h}_1 = 2\rho,$

$\mathrm{h}_2 = (\exp(\frac{\mu+\rho}{\tau}) - \exp(\mu - \rho))(\mu + \rho)(\mu - \rho)$

and

$\mathrm{h}_3 = 2(\rho(\exp(\frac{\mu+\rho}{\tau}) - \exp(\mu - \rho)) + \mu(1 - \exp(\mu - \rho))(1 - \exp(\frac{\mu+\rho}{\tau}))(\frac{1}{\rho-\mu} - \frac{\tau}{\rho+\mu})).$

Hence, Eq. (3.2.11) gives the relation between the power and the parameters μ, τ, λ and ρ. Now let us discuss the dependency of average power output of our generalized model on the parameters which characterize the model.

Figure 3.6 represents how the average power depends on an external static force where the other parameters are kept constant. The average power decreases monotonically as external load increases. As we have seen in the previous section of this chapter, the external load has a decreasing effect on particle current flowing from the hot reservoir to the cold reservoir (towards the positive x direction), in the domain where our model works as an engine. Consequently, the average power decreases with increasing external load.

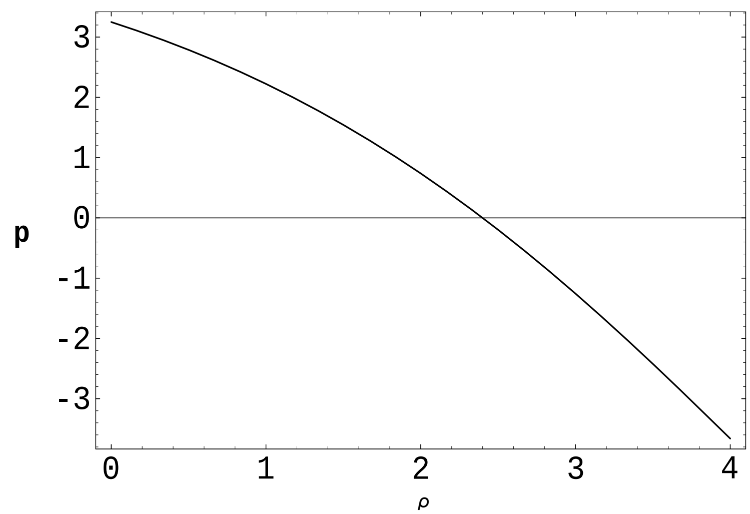

Figure 3.6: Plot of p versus ρ for $\lambda = 1$, $\mu = 4$, $\tau = 4$

The average power shows similar dependency on μ and τ as in the case where the external load is zero as shown in Figs. 3.7 and 3.8. However, the maximum attainable power decreases in the present case because of the relation between p and ρ shown in Fig. 3.6. The value of μ at which power attains its maximum value for the same value of τ and λ used in the case of zero external load increases if there is external load, i.e., maximum power point shifts to the right. For small values of μ (slightly greater than 0), p is negative because j is negative in this domain. But, since we want our model to function as an engine, we consider an interval in which $j > 0$. Accordingly, plots of p versus μ and p versus τ shown in Figs. 3.7 and 3.8 are plotted

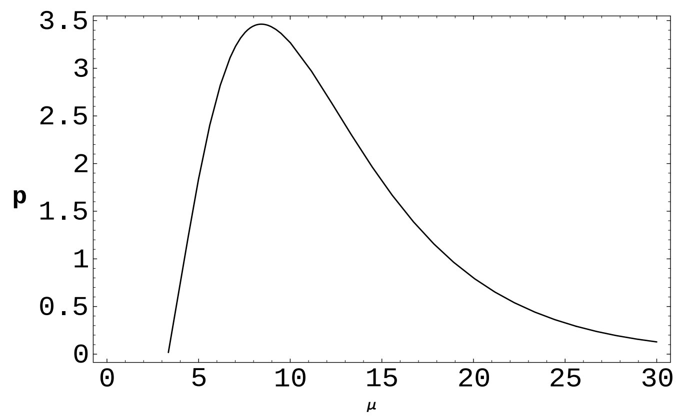

Figure 3.7: Plot of p versus μ for $\lambda = 1$, $\rho = 2$, $\tau = 4$

in the positive interval of j.

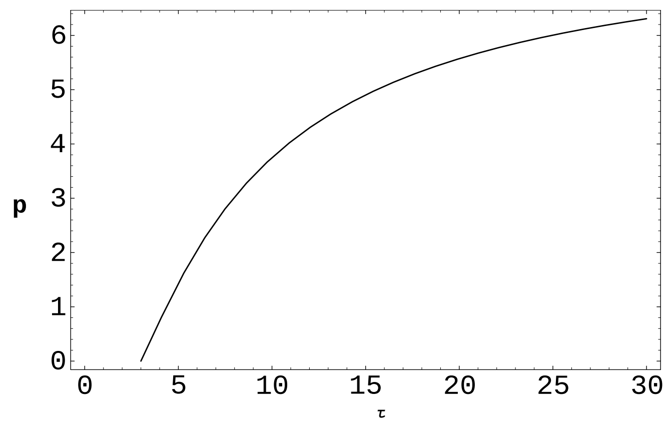

Figure 3.8: Plot of p versus τ for $\lambda = 1$, $\rho = 2$, $\mu = 4$

Finally, the efficiency (η) in the presence of static external force is defined as

$$\eta = \frac{W}{Q_h}. \tag{3.2.12}$$

Using Eqs. (3.2.4) and (3.2.5) into Eq. (3.2.13), η becomes

$$\eta = \frac{(\gamma v + f)(L_1 + L_2)}{\gamma v L_1 + U_o + f L_1 + \frac{1}{2}(T_h - T_c)}. \tag{3.2.13}$$

In terms of μ, τ and ρ (for $\lambda = 1$, i.e., without breaking the symmetry of the potential) η can be written as

$$\eta = \frac{H_1 H_3 + 2H_2}{H_2 + H_3 H_4}, \tag{3.2.14}$$

where

$\mathrm{H}_1 = 2\rho$,

$H_2 = (\exp(\frac{\mu+\rho}{\tau}) - \exp(\mu-\rho))(\mu+\rho)(\mu-\rho)$,

$H_3 = \rho(\exp(\frac{\mu+\rho}{\tau}) - \exp(\mu-\rho)) + \mu(1-\exp(\mu-\rho))(1-\exp(\frac{\mu+\rho}{\tau}))(\frac{1}{\rho-\mu} - \frac{\tau}{\rho+\mu})$

and

$H_4 = \frac{1}{2}(\rho-\tau)+\tau$.

Next we will look how the efficiency varies with changes in any one of the parameters.

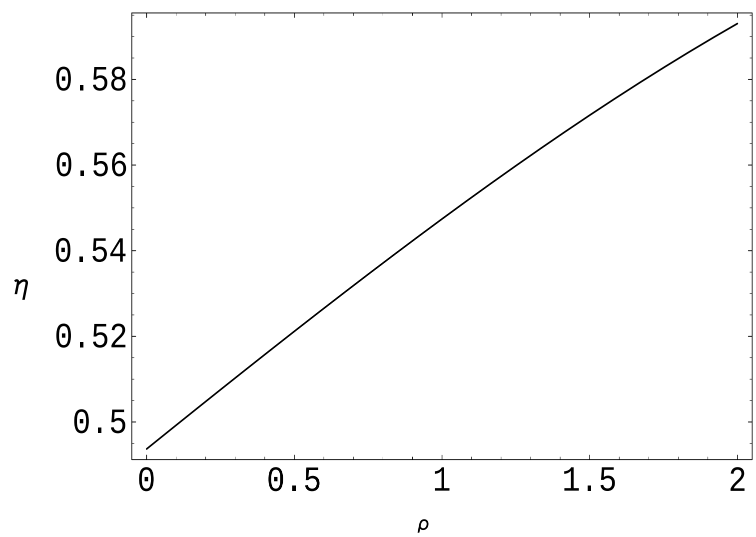

Figure 3.9: Plot of η versus ρ for $\lambda = 1$, $\tau = 4$, $\mu = 4$

From the plot of efficiency η versus static external force shown in Fig. 3.9, efficiency increases with the external static force linearly. In the presence of external load, useful work is done by the engine against the external load in addition to the work done we saw in section 2.3. As load increases more useful work is done against the load, hence, efficiency should increases with load. As the load is increased to the stall force (the force at which j vanishes), the efficiency tends to Carnot's efficiency.

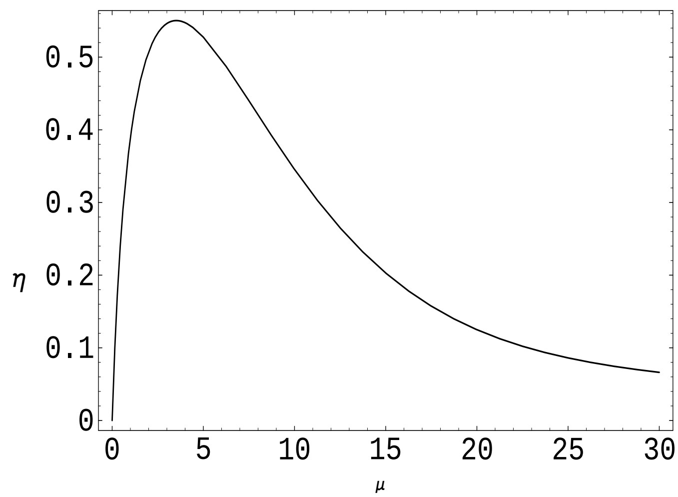

Figure 3.10: Plot of η versus μ for $\lambda = 1$, $\tau = 4$, $\rho = 1$

Figure 3.10 above is plot of efficiency η as a function of μ. In general the efficiency has similar property with respect to the parameter μ whether there is external load or not (compare Figs. 2.9 and 3.10). However, in the case of non-zero static external load, there is an increase in maximum efficiency because of the relation between efficiency and static external load shown in the plot of η versus ρ. See also Fig. 3.17 (maximum efficiency versus τ with and with out load).

Plot of η versus τ in the presence of static external load (see Fig. 3.11) also similar to Fig. 2.8 with zero external load taking thermal leakage in to account. However, the maximum efficiency increases in the presence of external load due to the increasing

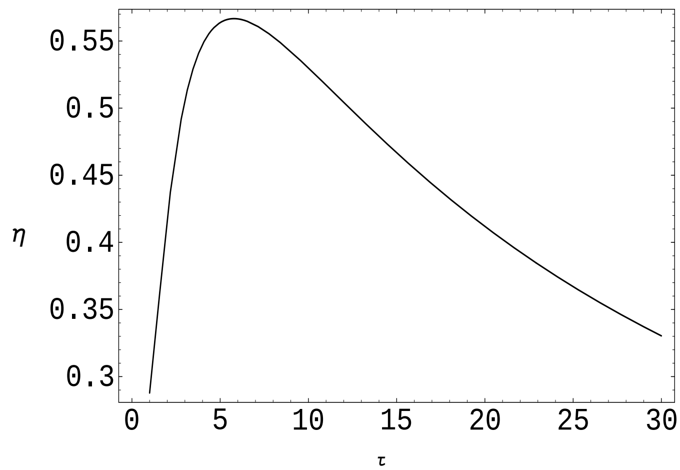

Figure 3.11: Plot of η versus τ for $\lambda = 1$, $\mu = 4$, $\rho = 1$

effect of load on efficiency as discussed earlier (see Fig. 3.9).

3.3 Maximum Power and Maximum Efficiency Regimes with Non-zero Load

Finally, the maximum power and maximum efficiency regimes of the generalized model are analyzed numerically. Maximum power output points μ_{mp} and maximum efficiency points $\mu_{m\eta}$, the values of μ at which power and efficiency attain their maximum values, respectively, which are functions of τ, λ and ρ are evaluated numerically. The maximum power output, $p(\mu_{mp})$, power out put at maximum efficiency point, $p(\mu_{m\eta})$, maximum efficiency, $\eta(\mu_{m\eta})$ and efficiency at maximum power output, $\eta(\mu_{mp})$, in the presence of static external load for symmetric saw-tooth potential (i.e., $\lambda = 1$) are also found and examined.

Maximum power point is obtained under the condition

$$\frac{\partial p}{\partial \mu}\Big|_{\mu=\mu_{mp}} = 0, \tag{3.3.1}$$

keeping the other parameters constant. Using the condition given in Eq. (3.3.1) into Eq. (3.2.11), gives the equation in appendix B (Eq. B.0.1) whose solution μ_{mp} is the value of μ at which the maximum power output is obtained. Similarly,

$$\frac{\partial \eta}{\partial \mu}\Big|_{\mu=\mu_{m\eta}} = 0, \tag{3.3.2}$$

keeping the other parameters constant, gives $\mu_{m\eta}$, the value of μ at which maximum efficiency is obtained. Using Eq. (3.3.2) into Eq. (3.2.15), the complex equation in appendix C (Eq. C.0.1) is obtained. Solution to Eq. C.0.1 $\mu_{m\eta}$ gives maximum efficiency point. Note that the same condition(s) and time step used in section 2.4 are used in this section also. Plot of μ_{mp} and $\mu_{m\eta}$ versus τ shows that, similar to Fig. 2.11, both μ_{mp} and $\mu_{m\eta}$ vary with τ linearly. Similar result was obtained for Feynman hot ratchet[28].

Substituting numerical solution of Eq. (B.0.1) of appendix B into Eq. (3.2.11) and Eq. (3.2.15) gives maximum power output and efficiency at maximum power output, respectively. Similarly, putting solution of Eq. (C.0.1) in appendix C into Eqs. (3.2.11) and (3.2.15), we obtain power output at maximum efficiency and maximum efficiency, respectively. Figure 3.13 shows plot of maximum power output $p_{mp}= p(\mu_{mp})$ and power output at maximum efficiency $p_{m\eta} = p(\mu_{m\eta})$ versus τ. Figure 3.14 shows maximum efficiency $\eta_{m\eta} = \eta(\mu_{m\eta})$ and efficiency at maximum power output

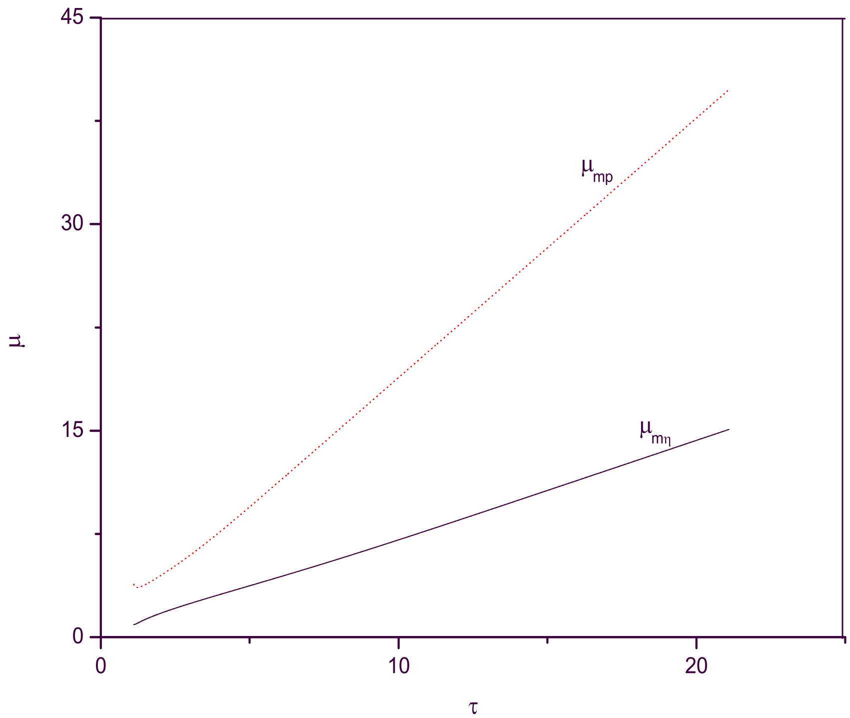

Figure 3.12: Plot of μ_{mp}, $\mu_{m\eta}$ for $\rho = 0.05$ versus τ.

$\eta_{m\eta} = \eta(\mu_{mp})$ versus τ. Here both power output and efficiency show the similar property as in the case of zero external load (See Figs. 2.12 and 2.13.)

Now let us look at the effect of external load on maximum power output, power at maximum efficiency, maximum efficiency and efficiency at maximum power output more closely comparing with the results of zero external load case.

Figure 3.15 is plot of μ_{mp} at $\rho = 0.05$, μ_{mp0} and $\mu_{m\eta0}$ versus τ. The plot shows that the maximum Power output point in the presence of non-zero constant external opposing load μ_{mp} is higher than the corresponding point with zero external load μ_{mp0}

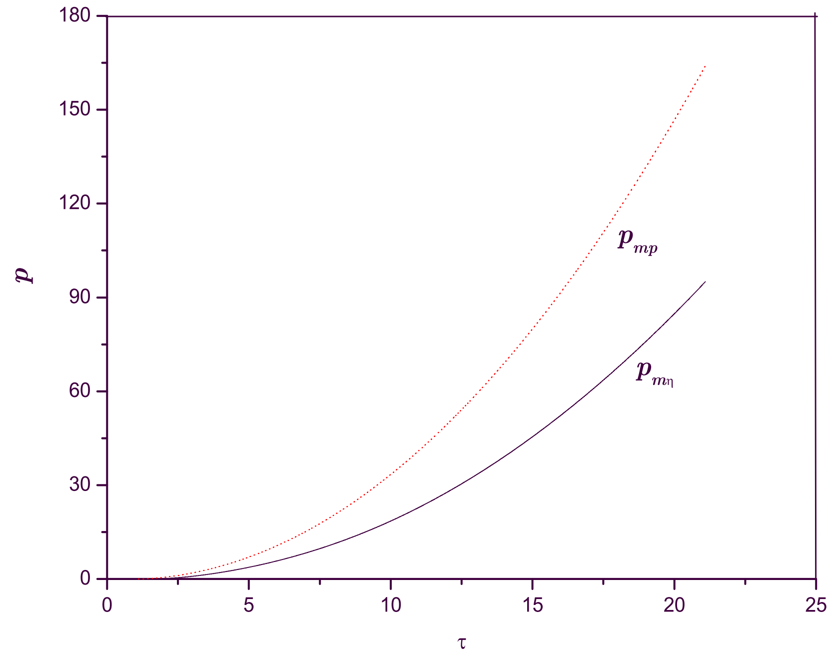

Figure 3.13: Plot of p_{mp} and $p_{m\eta}$ for $\rho = 0.05$ versus τ.

and maximum efficiency point with zero external load $\mu_{m\eta 0}$. Moreover, μ_{mp} increases at a constant rate higher than that of μ_{mp0} and $\mu_{m\eta 0}$ with respect to τ.

Numerical results of maximum power output with load $\rho = 0.05$, $p(\mu_{mp})$ and with out load, $p(\mu_{mpo})$, as well as power output at maximum efficiency with load $\rho = 0.5$, $p(\mu_{m\eta})$ and with out load, $p(\mu_{m\eta o})$ versus τ are shown in Fig. 3.16. For lower values of τ the power output at μ_{mp}, μ_{mpo} , $\mu_{m\eta}$ and $\mu_{m\eta o}$ is almost equal. For values of τ higher than some value, the power output is not the same at these points. Due to the opposing effect of external load on particle current from hot region to cold region in the positive x direction, the maximum power output and power output at

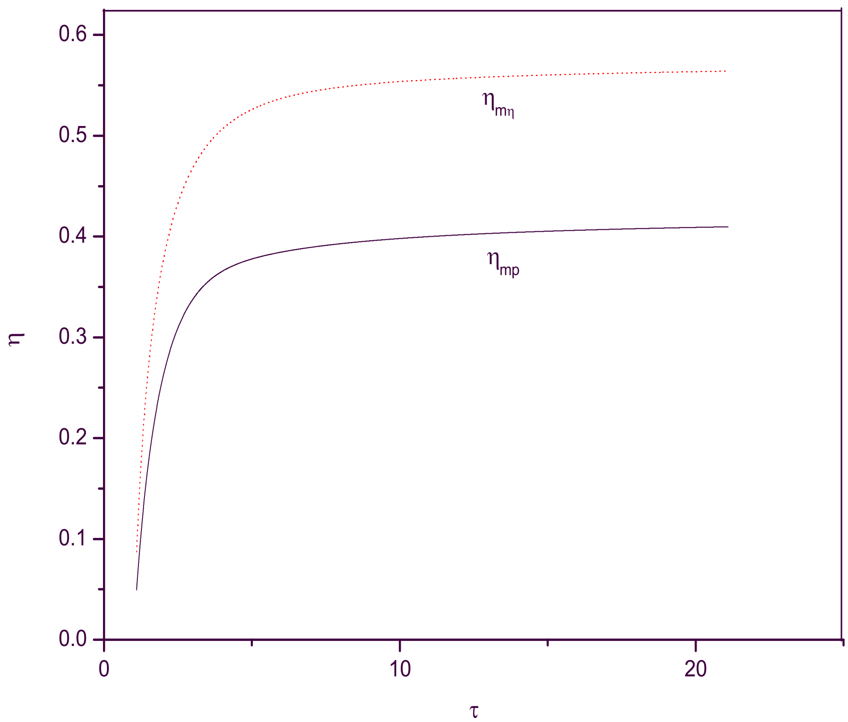

Figure 3.14: Plot of η_{mp} and $\eta_{m\eta}$ for $\rho = 0.05$ versus τ.

maximum efficiency decreases. Moreover, the external load has significant effect at the maximum power regimes than at the maximum efficiency regimes (see Fig. 3.16). A decrease in maximum power output due to the external load ($\rho = 0.05$) is higher than a decrease in power output at maximum efficiency due 10 times external load ($\rho = 0.5$). Moreover, if we look at Fig. 3.16 carefully, the real operation region of the power of the engine shrinks due to the presence of the external load.

Finally, we investigate the effect of load on efficiency at the maximum efficiency regimes and at the maximum power regimes. Figure 3.17 shows plot of maximum

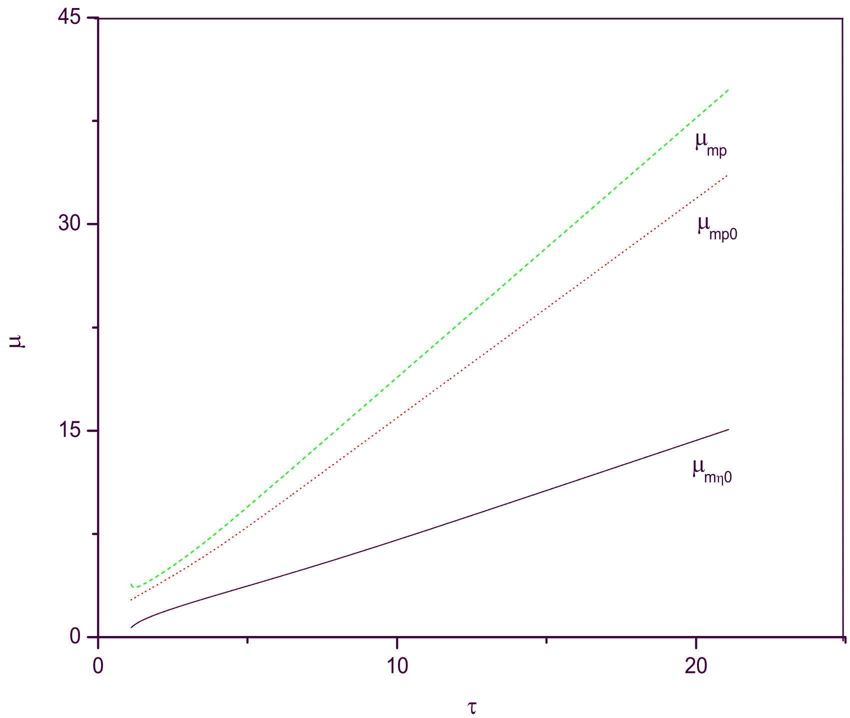

Figure 3.15: Plot of μ_{mp} (for $\rho = 0.05$), μ_{mp0} and $\mu_{m\eta 0}$ versus τ.

efficiency for the load $\rho = 0.5$, $\eta(\mu_{m\eta})$, maximum efficiency with out load, $\eta(\mu_{m\eta o})$, efficiency at maximum power output with load $\rho = 0.05$, $\eta(\mu_{mp})$ and efficiency at maximum power output with no load, $\eta(\mu_{mpo})$ versus τ. As we can see from the figure, the load has an increasing effect on maximum efficiency because of the relation between η and ρ shown in Fig. 3.9 but it has decreasing effect on efficiency at maximum power output due to the decreasing effect of load on power output (see Fig. 3.6) and hence on efficiency. In this case also, the effect of load at maximum power regimes is more significant than its effect at the maximum efficiency regimes. The

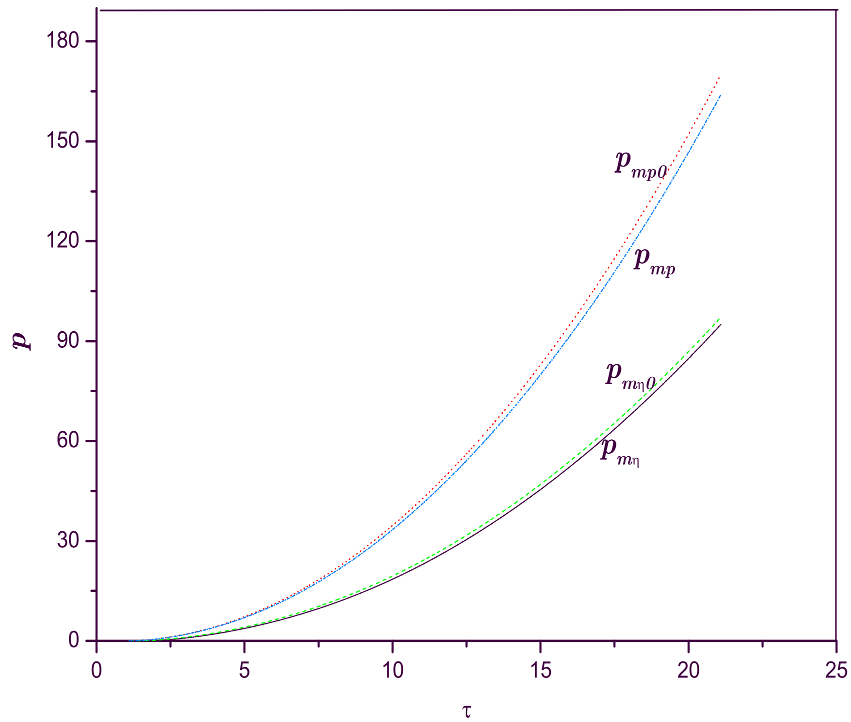

Figure 3.16: Plot of p_{mp} (for $\rho = 0.05$), p_{mp0}, $p_{m\eta}$ (for $\rho = 0.5$) and $p_{m\eta 0}$ versus τ.

factor by which efficiency decreased at maximum power output due to the external load $\rho = 0.05$ (change between curves $\eta(\mu_{mp})$ and $\eta(\mu_{mp0})$ in Fig. 3.17) is much higher than the factor by which maximum efficiency increased due to the effect of external load of $\rho = 0.5$ (change between curves $\eta(\mu_{m\eta})$ and $\eta(\mu_{m\eta}0)$ Fig. in 3.17). One can also see from Fig. 3.17, the real operation region of the engine expands in the presence of external load unlike that of power.

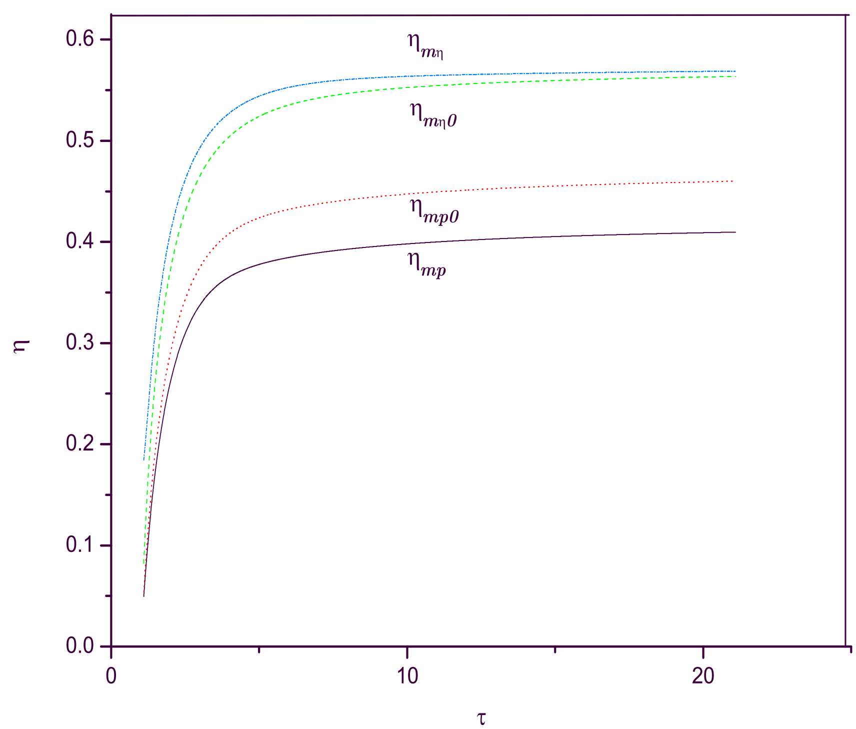

Figure 3.17: Plot of η_{mp} (for $\rho = 0.05$), η_{mp0}, $\eta_{m\eta}$ (for $\rho = 0.5$) and $\eta_{m\eta 0}$ versus τ.

Chapter 4

Summary and Conclusion

We have presented a simple stochastic model for a microscopic heat engine and studied some of its properties such as unidirectional current, power and efficiency in terms of the parameters μ ($\mu = \frac{U_o}{T_c}$), τ ($\tau = \frac{T_h}{T_c}$), λ ($\lambda = \frac{L_2}{L_1}$) and ρ ($\rho = \frac{fL_1}{T_c}$). To develop the model, a Brownian particle moving through a highly viscous medium in a periodic asymmetric saw-tooth potential and spatially varying temperature between two different constant values: hot temperature (T_h) and cold temperature (T_c) over a period which is the same as the period of the potential is used. In the absence of potential barrier ($\frac{U_o}{T_c}$) and external load, since the Brownian particle is equally probable to go to either direction in the space coordinate, the net particle current is zero. But, in the presence of potential barrier, due to temperature gradient, there is directed particle current from the hot reservoir to the cold reservoir (to the right). An analytic expression of probability current density for such directed particle current is found under two conditions (with and without static external load). Functional dependency of probability current density on the above parameters is analyzed for both conditions and compared. In particular, it is found that there is inverse linear relationship between the probability current density and the externally applied static force which acts in the direction opposite to the direction of flow of particle current.

The energetics of the engine is also studied by taking power and efficiency as objective functions for the above two conditions. Analytic expressions for power output and efficiency are obtained in terms of the parameters μ, τ, λ and ρ. Behaviour of power and efficiency with respect to the model parameters are investigated. Moreover, it is shown that power output decreases as the external static force increases monotonically. But, efficiency increases with the external static force linearly in the domain the external static force is less than the stalling force. The efficiency of our engine is compared with that of Carnot's efficiency: because of the thermal leakage (which can not be avoided) between the reservoirs, the engine never attains Carnot's efficiency.

Numerical results of power output and efficiency at maximum power regimes and maximum efficiency regimes as a function of τ are reported. It is also shown that as the external static force increases, maximum power points and maximum efficiency points (region in which heat engines operate [28]) approach each other.

The efficiency is sensitively dependent on model parameters. The energetic efficiency of an engine is not intrinsic property of the device and it depends on the characteristics of the imposed external load. Therefore, choosing the appropriate external load we can improve the efficiency considerably. The choice of appropriate potential profile also contributes lots in improving efficiency.

We have planned to develop simulations as an independent check to our present results in the near future.

Appendix A

Maximum efficiency points for $\rho = 0$

Solutions to Eq. (A.0.1) gives maximum efficiency points for zero external load where μ stands for $\mu_{m\eta o}$.

$$f_1(f_2 + f_3 - f_4 - f_5) - f_6 f_7 = 0, \tag{A.0.1}$$

where

$\mathrm{f}_1 = (-1 + \tau^2 + 2\mu + 2\mu\tau + \mu^2(\coth(\frac{\mu}{2\tau}) - \coth(\frac{\mu}{2}))),$

$\mathrm{f}_2 = 8(e^{\mu} - 1)(e^{\mu} - e^{\frac{\mu}{\tau}})(e^{\frac{\mu}{\tau}} - 1),$

$\mathrm{f}_3 = 4\mu(e^{\mu} - 1)(e^{\frac{\mu}{\tau}} - 1)(e^{\mu} - \frac{e^{\frac{\mu}{\tau}}}{\tau}),$

$\mathrm{f}_4 = 4\mu e^{\mu}(e^{\mu} - e^{\frac{\mu}{\tau}})(e^{\frac{\mu}{\tau}} - 1),$

$\mathrm{f}_5 = e^{\frac{\mu}{\tau}}(e^{\mu} - 1)(e^{\mu} - e^{\frac{\mu}{\tau}})\frac{4\mu}{\tau},$

$\mathrm{f}_6 = (2 + 2\tau + 2\mu(\coth(\frac{\mu}{2\tau}) - \coth(\frac{\mu}{2})) + \mu^2(\frac{1}{\tau(1-\coth(\frac{\mu}{\tau}))} + 0.5\,\mathrm{csch}(\frac{\mu}{2})^2)),$

and

$\mathrm{f}_7 = 4\mu(e^{\mu} - 1)(e^{\mu} - e^{\frac{\mu}{\tau}})(e^{\frac{\mu}{\tau}} - 1).$

Appendix B

Maximum power points for $\rho = 0.05$

Solutions to Eq. (B.0.1) gives maximum power points where there is external load ρ = 0.05 and μ stands for μ_{mp}.

$$g_1(g_2 + g_3 + g_4 + g_5 - g_6 - f_7 - g_8) - g_9(g_{10} + g_{11}) = 0, \qquad \text{(B.0.1)}$$

where

$$\mathrm{g}_1 = (\rho(e^{\frac{\mu+\rho}{\tau}} - e^{\mu-\rho}) + \mu(1 - e^{\mu-\rho})(1 - e^{\frac{\mu+\rho}{\tau}})(\tfrac{1}{\rho-\mu} - \tfrac{\tau}{\rho+\mu}))\tfrac{8e^{-2\rho}}{\tau},$$

$$\mathrm{g}_2 = -e^{\rho+\tau}\rho\tau(\rho(\tau - 1)(\mu + 1) - (\tau + 1)\mu(2 + \mu)),$$

$$\mathrm{g}_3 = e^{\frac{\rho(1+2\tau)+\mu}{\tau}}\rho(\rho(\tau - 1)(\mu + \tau) - (\tau + 1)\mu(2\tau + \mu)),$$

$$\mathrm{g}_4 = e^{\frac{(2+\tau)(\rho+\mu)}{\tau}}\rho(\rho(\tau - 1)(\tau + (2 + \tau)\mu) - (1 + \tau)\mu(2\tau + (2 + \tau)\mu)),$$

$$\mathrm{g}_5 = e^{\frac{2(\rho+\rho\tau+\mu)}{\tau}}(2\rho(\tau + 1)\mu(\mu + \tau) + 2\mu^3(2\tau + \mu) + \rho^2(\tau - \tau^2 - 4\tau\mu - 2(\mu - 1)\mu)),$$

$$\mathrm{g}_6 = e^{\frac{\rho+\mu(1+2\tau)}{\tau}}\rho(\rho(\tau - 1)(\tau + \mu + 2\mu\tau) - (\tau + 1)\mu(\mu + 2\tau(\mu + 1))),$$

$$\mathrm{g}_7 = e^{\frac{(\tau+1)(\mu+\rho)}{\tau}}2\mu(-\rho^2(\mu + \tau(2 + \mu)) + \mu^2(\mu + \tau(4 + \mu))),$$

$$\mathrm{g}_8 = e^{2\mu}\tau(2\rho(1 + \tau)\mu(1 + \mu) - 2\mu^3(2 + \mu) + \rho^2(1 + 2\mu(2 + \mu) - \tau(1 + 2\mu))),$$

$$\mathrm{g}_9 = 2(e^{\frac{\mu+\rho}{\tau}} - e^{\mu-\rho})(\mu-\rho)(\mu+\rho)(4e^{-\rho}(e^{\frac{\rho(1+\tau)+\mu}{\mu}} - e^{\mu})\mu^2 + \tfrac{4e^{-\rho}(e^{\rho}-e^{\mu})(e^{\frac{\rho+\mu}{\tau}}-1)\mu\rho(\rho(\tau-1)-(1+\tau)\mu)}{\rho^2-\mu^2}),$$

$$\mathrm{g}_{10} = 2\rho(\frac{e^{\frac{\mu+\rho}{\tau}}}{\tau} - e^{\mu-\rho}) + 2(1-e^{\mu-\rho})(1-e^{\frac{\mu+\rho}{\tau}})(\mu(\frac{1}{(\rho-\mu)^2} + \frac{\tau}{(\rho+\mu)^2}) + (\frac{1}{\rho-\mu} - \frac{\tau}{\rho+\mu}))$$

and

$$\mathrm{g}_{11} = -2e^{\mu-\rho}(1-e^{\frac{\mu+\rho}{\tau}})\mu(\frac{1}{\rho-\mu} - \frac{\tau}{\rho+\mu}) - \frac{2e^{\frac{\mu+\rho}{\tau}}(1-e^{\mu-\rho})\mu(\frac{1}{\rho-\mu} - \frac{\tau}{\rho+\mu})}{\tau}.$$

Appendix C

Maximum efficiency points for $\rho = 0.5$

Solutions to Eq. (C.0.1) gives maximum efficiency points where there is external load ρ= 0.5 and μ stands for $\mu_{m\eta}$.

$$h_1(h_3 + h_4 + h_5 h_6) - h_2(h_7 + h_8 + h_9 - h_{10}) = 0, \tag{C.0.1}$$

where

$$\mathrm{h}_1 = -(4e^{-\rho}(e^{\frac{\rho(1+\tau)+\mu}{\mu}} - e^{\mu})\mu^2 + \tfrac{4e^{-\rho}(e^{\rho}-e^{\mu})(e^{\frac{\rho+\mu}{\tau}}-1)\mu\rho(\rho(\tau-1)-(1+\tau)\mu)}{\rho^2-\mu^2}),$$

$$\mathrm{h}_2 = \tfrac{4e^{-\rho}}{\tau(\rho^2-\mu^2)^2}((e^{\frac{\mu+\rho}{\tau}} - e^{\mu-\rho})(\mu-\rho)(\mu+\rho) + (0.5(\tau-1)+\mu+\rho)((e^{\frac{\mu+\rho}{\tau}} - e^{\mu-\rho})\rho +$$
$$(1\text{-e}^{\mu-\rho}), (1 - e^{\frac{\mu+\rho}{\tau}})\mu(\tfrac{1}{\rho-\mu} - \tfrac{\tau}{\mu+\rho})))$$

$$\mathrm{h}_3 = (e^{\frac{\mu+\rho}{\tau}} - e^{\mu-\rho})(2\mu+\rho) + (\frac{e^{\frac{\mu+\rho}{\tau}}}{\tau} - e^{\mu-\rho})(\mu-\rho)(\mu+\rho),$$

$$\mathrm{h}_4 = (1 - e^{\mu-\rho})(1 - e^{\frac{\mu+\rho}{\tau}})\mu(\tfrac{1}{\rho-\mu} - \tfrac{\tau}{\mu+\rho}),$$

$$\mathrm{h}_5 = (0.5(\tau-1)+\mu+\rho)(\rho(\frac{e^{\frac{\mu+\rho}{\tau}}}{\tau} - e^{\mu-\rho}) + (1-e^{\mu-\rho})(1-e^{\frac{\mu+\rho}{\tau}})(\mu(\tfrac{1}{(\rho-\mu)^2} + \tfrac{\tau}{(\rho+\mu)^2}) +$$
$$(1\tfrac{}{\rho-\mu-\frac{\tau}{\rho+\mu})),}$$

$$\mathrm{h}_6 = (0.5(\tau-1)+\mu+\rho)(-e^{\mu-\rho}(1 - e^{\frac{\mu+\rho}{\tau}})\mu(\tfrac{1}{\rho-\mu} - \tfrac{\tau}{\rho+\mu}) - \frac{e^{\frac{\mu+\rho}{\tau}}(1-e^{\mu-\rho})\mu(\frac{1}{\rho-\mu}-\frac{\tau}{\rho+\mu})}{\tau}),$$

$$\mathrm{h}_7 = e^{\rho}\rho^2\tau(\rho^2(\tau-1) - 2\rho(\tau+1)\mu + (\tau-1)\mu^2),$$

$$\mathrm{h}_8 = e^{\frac{\rho+\mu(1+\tau)}{\tau}}\rho((1+\tau)^2\mu^4 - \rho(\tau-1)\mu^2(\tau(\mu-1)+\mu) + \rho^3(\tau-1)(\mu+\tau+\mu\tau) -$$
$$\rho^2(\tau+1)\mu(\mu+\tau(2+\mu))),$$
$$\mathrm{h}_9 = e^{\mu}\tau(-\rho(1+\tau)\mu^4 + \rho^3(1+\tau)\mu(2+\mu) + \mu^5(2+\mu) + \rho^4(1-\tau(1+\mu)+\mu(3+$$
$$\mu)) - \mu^2\rho^2(-1+\tau-\mu\tau+\mu(5+2\mu)))$$

and

$$\mathrm{h}_{10} = e^{\frac{\rho(1+\tau)+\mu}{\tau}}(\rho(1+\tau)\mu^4 - \rho^3(1+\tau)\mu(2\tau+\mu) + \mu^5(2\tau+\mu) + \mu^2\rho^2((\tau-1)\tau+\mu-$$
$$5\mu\tau-2\mu^2) + \rho^4(\tau^2+(\mu-1)\mu+\tau(3\mu-1))).$$

Bibliography

[1] Peter Reimann, Physics Report, **361** (2002) 57-265.

[2] Peter H*ä*nggi, Fabio Marchesoni, and Franco Nori, Ann. Phys. (Leipzig) **14**, No. 1-3, 51-70 (2005).

[3] R. Dean Astumian, Science, vol. **276** (1997).

[4] Ken Sekimoto, arxiv: cond-mat/9611005 v**1** 1996.

[5] R. Dean Astumian and Peter H*ä*nggi, Physics Today (2002).

[6] Martin Bier, Phys. Rev. Lett. **91**, 14 (2003).

[7] Imre Der*é*nyi, Martin Bier, and R. Dean Astumian, Phys. Rev. Lett. **83**, 5 (1999).

[8] Terence Strick, Jean-Francois Allemand, Vincent Croquette, and David Bensimon, Physics Today (2001).

[9] P. Reimann and P. H*ä*nggi, Appl. Phys. A**75**, 169-178 (2002).

[10] Frank J*ü*licher, Armand Ajdari and Jacques Prost, "Reviews of Modern Physics", vol. **69**, No. 4 (1997).

[11] R. P. Feynman, R. B. Leighton and M. Sands, "The Feynman Lectures on Physics", **vol. I**, Chap. 46 (Addison-Wesley Publ. Co., Reading, Massachussets, 1963).

[12] Juan M. R. Parrondo: "Criticism of Feynman's analysis of the ratchet as an engine", (1996).

[13] Marcelo O. Magnasco, Phys. Rev. Lett. **71**, 10 (1993).

[14] Ken Sekimoto, Journal of the Physical Society of Japan, vol. **66**, No. 5 (1997) pp. 1234-1237.

[15] Ken Sekimoto, "Progress of Theoretical Physics Supplement", No. 130 (1998).

[16] Mesfin Asfaw and Mulugeta Bekele, Phys. Rev. E**72**, 056109 (2005).

[17] Morten Ø. Jensen, Sanghyun Park, Emad Tajkhorshid, and Klaus schulten, Pnas, vol. **99**, No. 10 (2002) 6731-6736.

[18] Marcin Kostur, Lukasz Machura, Peter Hänggi, Jurek Luczka and Peter Talkner, arxiv: cond-mat/0512152 **v1** (2005).

[19] Yu. A. Makhnovskii, V. M. Rozenbaum, D.-Y. Yang and S. H. Lin, Phys. Rev. E **69**, 021102 (2004).

[20] Mesfin Asfaw and Mulugeta Bekele, Eur. Phys. J. B **38**, 457-461 (2004).

[21] Carlos Bustamante, Jan Liphardt, Felix Ritort: "The Nonequilibrium Thermodynamics of Small Systems."

[22] Paul Grayson, Emad Taikhorshid, and klaus schulten, Biophysical Journal volume **85** 2003 36-48.

[23] Benoit Roux and Klaus schulten, Structure, vol. **12**, 1343-1351, 2004.

[24] Anatoly B. Kolomeisky and Michael E. Fisher, Biophysical Jounal volume **84** 2003 1642-1650.

[25] Imre Derényi and Tamas Vicsek, Proc. Natl. Acad. Sci. USA vol. **93**, pp. 6775-6779, 1996.

[26] Deyu Lu, Paul Grayson, and Klaus Schulten, Biophysical journal Volume **85**, (2003) 2977-2987.

[27] Ioan Kosztin and Klaus Schulten, PRL **93**, 238102 (2004).

[28] S Velasco, J M M Roco, A Medina and A Calvo Hernández, J. Phys. D: Appl. Phys. **34** (2001) 1000-1006.

[29] C. W. Dardiner: " Handbook of Stochastic Methods" 2nd ed. (Springer-Verlag, Berlin, 1990) Chap. 4.

[30] M. O. Magnaso, Europhys. Lett., **33** (8), pp. 583-588 (1996).

DECLARATION

I hereby declare that this thesis is my original work and has not been presented for a degree in any other University. All sources of material used for the thesis have been duly acknowledged.

Name: ***Demmelash Hailu***

Signature:_______________

This thesis has been submitted for examination with my approval as University advisor.

Name: ***Dr. Mulugeta Bekele***

Signature:_______________

Addis Ababa University

Department of Physics

June, 2006.